International Journal of Heat and Mass Transfer 185 (2022) 122248

Contents lists available at ScienceDirect

International Journal of Heat and Mass Transfer

journal homepage: www.elsevier.com/locate/hmt

Thermal boundary layer of laminar flow of dilute polymer solution

Saeed Parvar[a,b,1,*], Carlos B. da Silva[c], Fernando Pinho[a]

[a] CEFT/FEUP, Universidade do Porto, Rua Dr. Roberto Frias, Porto 4200-465, Portugal
[b] INEGI, Campus da FEUP, Rua Dr. Roberto Frias, Porto 4200-465, Portugal
[c] LAETA, IDMEC, Instituto Superior Técnico, Universidade de Lisboa, Lisboa, Portugal

ARTICLE INFO

Article history:
Received 30 June 2021
Revised 3 November 2021
Accepted 9 November 2021
Available online 2 January 2022

Keywords:
Approximate local self-similar solution
Thermal boundary layer flow
Viscous dissipation
Viscoelastic fluids
FENE-P constitutive equation

ABSTRACT

The thermal boundary layer flow is a canonical flow with characteristics that are present in most natural and industrial convection flows. An approximate self-similar solution is proposed for the first time for the thermal boundary layer of steady laminar flow of viscoelastic fluids, described by the finitely extensible nonlinear elastic constitutive equation with Peterlin's closure (FENE-P model). This semi-analytical thermal solution is obtained by performing an order of magnitude analysis and ensuing simplifications of the governing equations by assuming that the fluid properties are independent of temperature therefore decoupling the flow governing equations from the energy equation. The effects of viscoelasticity quantified with the Weissenberg number based on the streamwise coordinate (x) (Wi_x) up to $Wi_x = 1$ and viscous dissipation (results are presented for Brinkman numbers between -40 and +40) on thermal boundary layer characteristics are investigated comprehensively for both constant wall temperature and constant wall heat flux. At low elasticity levels ($Wi_x < 0.01$) the solution exhibits a global self-similar behavior in which flow and thermal quantities collapse on the corresponding Newtonian curves, and the polymer characteristics show a unique behavior if adequately normalized. However, by increasing flow elasticity the unique self-similar behavior of the approximate solution is lost, with the elasticity dependent results exhibiting local variations. In addition, the effects of elasticity are intensified by viscous dissipation. For the present study cases, it is observed that elasticity may change Nusselt numbers by more than 8%, and the thermal boundary layer thickens by up to 10%.

1. Introduction

Heat transfer in viscoelastic flows is relevant for applications in thermal science. Under turbulent flow conditions, where polymer solutions exhibit intense drag reduction [1], the concomitant heat transfer reduction can reduce the effectiveness of heat transfer, and this has both disadvantages as well as advantages depending on the application [2–7]. Turbulent flows, by the typical range of their Reynolds numbers, lead to the formation of boundary layers. However, of concern to this work are high Reynolds number boundary layer flows in the laminar regime, which are easily found because the addition of polymers, or other additives like surfactants, that impart viscoelastic behavior to the otherwise Newtonian solvent, raises the viscosity of the solutions. Of interest are dilute or semi-dilute polymer or surfactant solutions that are not excessively viscous to allow sufficiently high Reynolds number flows, but since they are more viscous than the solvent there might still be some effects of viscous dissipation [8]. However, if the range of temperatures in the flow is not too large the assumption of temperature independent fluid properties provides sufficiently accurate solutions while significantly simplifying the solution from a mathematical perspective, as discussed in [9–11]. The available literature concerning the thermal behavior of boundary layer flows of viscoelastic fluids is rather limited as reviewed next, hence the current contribution.

Early studies on thermal boundary layer flows with non-Newtonian fluids involve inelastic fluids as in Massoudi [12], who studied the heat transfer of a power law fluid in the laminar boundary layer flow over a wedge. Power law fluids were also considered by Khan et al. [13] who utilized the integral von Kármán-Pohlhausen approach to study the heat transfer in flows over circular cylinders, but restricted their analysis to sufficiently low Reynolds numbers to allow laminar flow in the whole domain: they reported drag reduction and heat transfer enhancement due to shear-thinning. Shokouhmand and Soleimani [14] investigated the heat transfer over a moving flat plate of power-law fluids while considering arbitrary injection/suction and viscous dissipation. They showed the large impact of viscous dissipation in heat

* Corresponding author at: CEFT/FEUP, Universidade do Porto, Rua Dr. Roberto Frias, Porto 4200-465, Portugal.
E-mail address: parvar@kth.se (S. Parvar).
[1] Present address : SeRC and FLOW, Engineering mechanics, KTH Royal Institute of Technology, SE-10044 Stockholm, Sweden.

https://doi.org/10.1016/j.ijheatmasstransfer.2021.122248
0017-9310/

Nomenclature

Latin letter

Br	Brinkman number (-)
C_i	dimensionless coefficients (-)
C_{ij}	conformation tensor (-)
c_p	specific heat ($J \cdot kg^{-1} \cdot K^{-1}$)
$f(C_{kk})$	Peterlin function (-)
$f_e(L)$	second scalar function of L (-)
f_x, f_y	expansion/contraction factors of the mesh (-)
G	similarity function of momentum (-)
h_x	local convection coefficient ($W.m^{-2}.K^{-1}$)
K	similarity function of Peterlin function (-)
L	dumbbell maximum extensibility (-)
$\mathcal{L}$	length of the flat plate (m), cf. Figure 1
n_x,n_y, n_z	number of grid points in the x, y, z directions (-)
Nu	Nusselt number (-)
P	pressure (Pa)
Pr	Prandtl number (-)
q_w	constant wall heat flux ($W.m^{-2}$)
Re	Reynolds number (-)
$\|S\|$	norm of the strain rate tensor (s^{-1})
S_{ij}	strain rate tensor (s^{-1})
T	temperature (K)
T_w	constant wall temperature (K)
T_∞	temperature of free stream flow (K)
u,v,w	velocity in streamwise, normal, and spanwise directions ($m.s^{-1}$)
u_i	velocity vector ($m.s^{-1}$)
U_∞	free stream flow velocity ($m.s^{-1}$)
Wi	Weissenberg number (-)
x_i	the i*th* space coordinate (m)
x, y	streamwise and transverse/cross-stream coordinates (m)

Greek letter

α	fluid thermal diffusivity ($m^2.s^{-1}$)
α^*	energy partitioning coefficient (-)
β_p	ratio of kinematic viscosities (-)
δ_{ij}	Kronecker delta
δ_u	dynamic boundary-layer thickness (m)
δ_T	thermal boundary-layer thickness (m)
Δx,Δy, Δz	grid spacing in the x, y, z directions (m)
η	dimensionless cross-stream coordinate (-)
θ	dimensionless temperature (-)
λ	relaxation time of polymer (s)
ρ	fluid density ($kg.m^{-3}$)
τ_{ij}	total stress tensor (Pa)
τ_{ij}^P	polymer stress tensor (Pa)
τ_{ij}^S	solvent stress tensor (Pa)
υ_0	the zero-shear rate kinematic viscosity ($m^2.s^{-1}$)
υ_p	polymer kinematic viscosity ($m^2.s^{-1}$)
υ_s	solvent kinematic viscosity ($m^2.s^{-1}$)
ψ	the stream function ($m^2.s^{-1}$)

Subscripts and superscripts

$[s]$	refers to solvent
$[p]$	refers to polymer
x	refers to local value
$\mathcal{L}$	refers to whole plate
∞	refers to free stream

transfer, especially when velocity gradients are large, which can cause a reversal of the wall heat flux and substantial variations in Nusselt number. Other additional analytical works on heat transfer in the presence of viscous dissipation, and showing its strong impact in various different canonical flows, such as pipe [15], fixed parallel plates [16], and Couette–Poiseuille flows [17] involve again the power law fluid, i.e., a fluid model devoid of elastic effects. Regarding the thermal boundary layer flows of viscoelastic fluids over flat surfaces, Olagunju [18] investigated the specific case of Falkner-Skan flows with constant wall temperature and viscous dissipation for the finitely extensible nonlinear elastic constitutive equation with Peterlin's closure (henceforth called FENE-P model). In his investigation, although he only used the fluid shear stress in the approximate momentum equation, the corresponding polymer contribution was affected by his neglect of the full advection terms in the simplified constitutive equation calculating the conformation tensor. An increase in the elasticity level reduced the skin friction and enhanced heat transfer.

More recently, Benzi et al. [19,20] studied the thermal laminar boundary layer flow of Oldroyd-B and FENE-P fluids, respectively, again for a constant wall temperature but without considering viscous dissipation effects, and for other forms of Peterlin's functions [21,22]. Their solution was also an approximate similarity solution [23–28] that depended on local Reynolds and Weissenberg numbers. Benzi et al. [20] used the shear component of the conformation tensor to compute a position-dependent effective viscosity, but the advection term of the conformation tensor considered by Benzi et al. [20] lead to some unphysical results of their effective viscosity near the free stream region. To fix that, they used an elaborate mathematical simplification to obtain the physical solution. Although they could obtain the peak values of polymer stress, they used different polymer characteristics in their simulations and could not precisely calculate the polymer stresses near the wall, which effectively prevents the use of their solution for validation purposes. It is worth mentioning that neither Olagunju [18] nor Benzi et al. [20] investigated in a complete form the effect of elasticity on thermal layer thickness and in addition they did not investigate the thermal case with imposed wall heat flux. It is also noteworthy that there are also some other analytical studies about the effect of viscoelasticity and viscous dissipation on heat transfer of viscoelastic fluid described, for instance by the simplified form of the Phan-Thien–Tanner constitutive equation (PTT) as in fully-developed pipe [29] or channel flow [30] for which a complete analytical solution can be obtained without the need for simplifications on account of the simpler geometries. Such fully-developed solutions can actually be adapted for some forms of the FENE-P model following the idea of Oliveira [31], but their fully-developed nature and ensuing simplicity makes them somehow out of scope for the present study.

Since we are dealing with fluid flows in the liquid phase, the momentum equation is uncoupled from the energy equation through the assumption of temperature independent fluid properties, the main issue in the investigation of heat transfer of viscoelastic fluids is essentially the accurate solution of the flow governing equations. To obtain the appropriate solution a large Reynolds number (Re) is required and $Re/Wi \gg 1$ is also verified, where Wi is the Weissenberg number defined as the ratio of elastic over viscous forces. These conditions were reported by Rajagopal et al. [32] in their investigation of Falkner-Skan flows of second order fluids. In addition, Olagunju [18,33] found that the approximate similarity solution of laminar boundary layer flow of FENE-P fluid remains dependent on local coordinates, in contrast to the corresponding approximate similarity solution for Newtonian fluids, except in the limit of low elasticity behavior [34].

While studying boundary layer-type flows of viscoelastic fluids, Parvar et al. [35–37] observed that Olagunju [18,33] had neglected some non-negligible terms in his final simplified constitutive equation that distorted the prediction of some polymer stress components and could affect velocity profiles at large elasticity, while

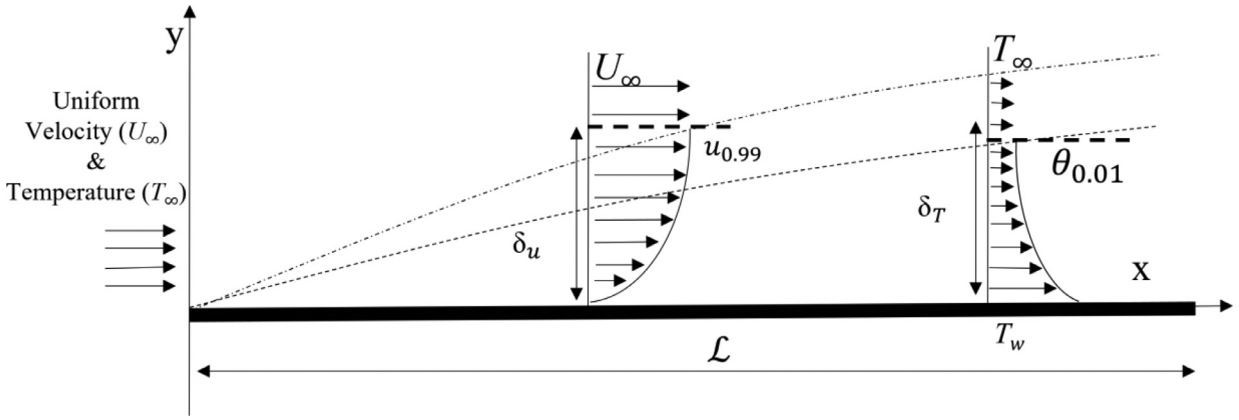

Fig. 1. Schematics of the flat plate flow with definitions of dynamic and thermal boundary layer thicknesses and coordinate system.

reducing the range of validity of his solution. The more precise simplifications of the constitutive equation by Parvar et al. [35–37] for the planar jet and boundary layer flows allowed for improved and more complete solutions that remained valid up to larger Weissenberg numbers than in Olagunju [18] and form the basis of the current contribution. In the present study, similar to Olagunju [18,33] and Benzi et al. [19,20], again only the total fluid shear stress is considered in the final simplified approximate momentum equation, but the more relevant advection terms of the conformation tensor evolution equations are considered and the equations derived are for general Peterlin functions. Nevertheless, the numerical results presented pertain to a specific set of Peterlin functions for better understanding and to facilitate comparison with Olagunju's solution [18,33]. In addition to a more accurate thermal solution for the constant wall temperature condition, the case for a constant wall heat flux is included here and in both cases due account is taken of stress work effects on the thermal energy equation. These are necessary because polymers solutions are typically more viscous than the (single) Newtonian solvent solutions.

The main aim of the present work is to obtain a semi-analytical solution to study and improve our understanding of the thermal boundary layer characteristics of viscoelastic polymer solution flows. In particular, this result will assist us to investigate the combined effects of viscoelasticity and viscous dissipation on heat transfer characteristics as for Newtonian fluids [40,41]. The semi-analytical solution is also a useful tool for validation purposes and to benchmark results when developing computational codes for viscoelastic fluid flow and heat transfer.

This work starts with the planar laminar boundary layer flow solution of Parvar et al. [37] for FENE-P fluids, which was also verified against predictions by the RheoFoam toolbox of the freeware OpenFoam code [38,39] and proceeds to the corresponding thermal boundary layer flow problem through the solution of the energy equation.

After presenting the flow setup and coordinate system in Section 2, the full set of governing equations are presented in Section 3, then the assumptions and corresponding simplifications for each flow case are discussed in Section 4, leading to the final set of simplified equations. The numerical methods used to solve them are given in Section 5 and their results and discussion are the subject of Section 6.

2. Flow setup

Fig. 1 shows the schematics of the two-dimensional laminar thermal boundary layer flow over a flat plate under conditions of zero pressure gradient. A free stream of uniform velocity (U_∞) and temperature (T_∞) flows over a thin motionless semi-infinite flat plate of length $\mathcal{L}$, which is either at a constant temperature (T_w) or subject to a constant wall heat flux (q_w). The dynamic and thermal boundary-layer thicknesses are δ_u and δ_T, respectively. The origin of the coordinate system is located at the plate leading edge, with x, y denoting the streamwise and transverse/cross-stream coordinates, respectively. No-slip and no temperature jump boundary conditions are imposed at the wall. The fluid velocity increases with wall distance across the boundary layer and the temperature varies according to thermal conditions with both approaching asymptotically the free-stream velocity and temperature values [38,39].

The dynamic boundary-layer thickness (δ_u) is defined as the transverse distance from the wall to a location where the local streamwise velocity equals 99% of the free stream velocity. To define the thermal boundary layer thickness, it is necessary to introduce first a dimensionless temperature θ which depends on the wall thermal boundary conditions as explained in Section 3.2. In any case, the thermal boundary layer thickness (δ_T) is defined as the transverse distance from the wall to the location of $|\theta(\eta)| = 0.01$ (negative and positive values of θ may exist for some cases with viscous dissipation), where η is an adequate dimensionless cross-stream coordinate yet to be defined.

3. Governing equations

To describe the rheology of the viscoelastic fluids the finitely extensible nonlinear elastic model with Peterlin's closure (FENE-P) [9,42] was adopted. This kinetic theory based constitutive equation is used for dilute polymer solutions and provides the main ingredients of viscoelasticity such as memory effects, shear-thinning behavior, shear-dependent normal stresses and bounded elastic stresses. Although the original FENE-P model depends on temperature, it is assumed that temperature variations are small enough to consider a simpler temperature independent version of the FENE-P model [9–11].

The governing equations are presented next in Einstein's notation. The conservation of mass for incompressible fluids is

$$\frac{\partial u_k}{\partial x_k} = 0, \tag{1}$$

and the Cauchy equation is written as

$$\rho\left(\frac{\partial u_i}{\partial t} + u_k\frac{\partial u_i}{\partial x_k}\right) = -\frac{\partial P}{\partial x_i} + \frac{\partial \tau_{ik}}{\partial x_k}, \tag{2}$$

where u_i is the velocity vector, P is the pressure and ρ is the fluid density. The fluid total extra stress τ_{ij} is given by

$$\tau_{ij} = \tau_{ij}^{s} + \tau_{ij}^{p}, \tag{3}$$

the sum of the Newtonian solvent stress (τ_{ij}^{s}) with the polymer stress (τ_{ij}^{p}). The Newtonian solvent stress tensor is written as

$$\tau_{ij}^{s} = 2\rho\upsilon_s S_{ij}, \tag{4}$$

where υ_s is its kinematic viscosity and S_{ij} is the rate-of-strain tensor defined by

$$S_{ij} = \frac{1}{2}\left(\frac{\partial u_i}{\partial x_j} + \frac{\partial u_j}{\partial x_i}\right). \tag{5}$$

The polymer stress tensor is given by the FENE-P model, here written as

$$\tau_{ij}^{p} = \frac{\rho\upsilon_p}{\lambda}\left[f(C_{kk})C_{ij} - f_e(L)\delta_{ij}\right], \tag{6}$$

where υ_p is the zero shear rate polymer kinematic viscosity coefficient, λ is the relaxation time, δ_{ij} is the identity tensor, C_{ij} is the dimensionless conformation tensor, $f(C_{kk})$ is a scalar function known as Peterlin's function, that depends on the trace of the conformation tensor and on the square of the maximum normalized dumbbell extensibility (L^2) and $f_e(L)$ is a second scalar function of L. Several variants of the FENE-P model are presented in the literature, however, by considering $L^2 \gg 3$ they essentially provide identical results. Three of those models are given by

$$f(C_{kk}) = \frac{L^2}{L^2 - C_{kk}} \text{ and } f_e(L) = 1, \tag{7-a}$$

$$f(C_{kk}) = \frac{L^2}{L^2 - C_{kk}} \text{ and } f_e(L) = \frac{L^2}{L^2 - 3}, \tag{7-b}$$

$$f(C_{kk}) = \frac{L^2 - 3}{L^2 - C_{kk}} \text{ and } f_e(L) = 1. \tag{7-c}$$

The first set of functions is considered as the original form, but was modified by Bird et al. [42] who used Eq. (7-b) as discussed in Beris and Edwards [8]. The third variant has also been used in particular to study turbulent flows of polymer solutions such as in direct numerical simulations [43–46], and in turbulence modeling for large eddy simulations [47,48] and Reynolds-averaged Navier–Stokes simulations [49–51]. In the present investigation the mathematical formulations are general and independent of the set of functions, but the presented numerical results are for the third variant (Eq. (7-c)).

In kinetic theory based constitutive equations the connector force within the dumbbells depends on fluid temperature, but its influence is null for isothermal flows and negligible if the temperature variation is not too large. Also the relaxation time and viscosity coefficients of the polymer may depend on temperature, especially for temperatures that are within 100 K of the glass temperature, but all these are excluded from our analysis.

To close the polymer model, the conformation tensor is described by the following evolution equation

$$\frac{\partial C_{ij}}{\partial t} + u_k\frac{\partial C_{ij}}{\partial x_k} = C_{jk}\frac{\partial u_i}{\partial x_k} + C_{ik}\frac{\partial u_j}{\partial x_k} - \frac{1}{\lambda}\left[f(C_{kk})C_{ij} - f_e(L)\delta_{ij}\right] \tag{8}$$

Finally, the general form energy equation, is

$$\rho c_p\left(\frac{\partial T}{\partial t} + u_k\frac{\partial T}{\partial x_k}\right) = \frac{\partial}{\partial x_k}\left(k\frac{\partial T}{\partial x_k}\right) + \tau_{ik}\frac{\partial u_i}{\partial x_k}, \tag{9}$$

in which T is the temperature, k is the thermal conductivity, c_p is the specific heat and ρ is density. The second term on the right-hand side of Eq. (9) is the viscous dissipation term that partially accounts for entropic elastic effects of the polymer and therefore contributes to temperature changes (Peters and Baaijens [52]). Through the split of the total fluid stress into solvent and polymer contributions on the last term on the right-hand-side, with the polymer stress contribution multiplied by the energy partitioning coefficient α^*, and an additional term on the right-hand-side, one could also consider the effects of the energy stored elastically as internal energy. This elastically stored energy would not contribute to temperature changes but could be released in other flow locations, i.e., different from the locations where energy is stored.

Sarti and Esposito [53] have experimentally shown that for some polymer melts (and naturally less so for dilute polymer solutions), only the viscous dissipative term matters when we are well above the glass temperature and therefore $\alpha^* = 1$. Peters and Baaijens' [52] calculations showed the negligible impact of the need to account for both elasticity effects unless the Weissenberg number becomes very high and even then those effects are not very intense. However, under very high Weissenberg number flow conditions the approximate dynamic boundary layer flow solution, upon which this thermal solution is based, breaks down. In conclusion, the thermal energy Eq. (9) used here is adequate for the range of validity of this work, to be discussed in the results section, which does not extend to very high Weissenberg number flows. Nevertheless, note that this form of the energy equation was also utilized by Wachs and Clermont [54] to study heat transfer in flows at large Weissenberg numbers and Pimenta and Alves [11] in developing the RheoFoam toolbox of OpenFoam [40,41].

3.1. The simplified governing equations

The procedure of simplifying the governing equations for isothermal boundary layer type flows of FENE-P fluids was carried out in detail by Parvar et al. [35–37]. Therefore, in the following, those steps are briefly summarized and adapted to include the simplification of the thermal energy equation.

The momentum equation in the streamwise direction (x) and the energy equation are simplified considering that the streamwise gradients of stress and heat flux are negligible in comparison to the transverse gradients, i.e., $\partial\tau_{xx}^{s}/\partial x << \partial\tau_{xy}^{s}/\partial y$, $\partial\tau_{xx}^{p}/\partial x << \partial\tau_{xy}^{p}/\partial y$, and $\partial^2 T/\partial x^2 << \partial^2 T/\partial y^2$. Furthermore, the analysis of the y-momentum equation leads to negligible $\partial p/\partial y$, and since the flow of interest to this work has a free stream with $dp_\infty/dx = 0$, there is no need to consider further the pressure gradients and to solve the y-momentum equation.

The zero-shear rate kinematic viscosity (ν_0) of the solution is the sum of the solvent and polymer kinematic viscosities defining the following ratio of viscosities (β_p) as

$$\beta_p = \frac{\nu_p}{\nu_s + \nu_p} = \frac{\nu_p}{\nu_0}. \tag{10}$$

At this stage it is beneficial to introduce the Reynolds number ($Re_{\mathcal{L}}$) of the plate,

$$Re_{\mathcal{L}} = \frac{U_\infty \mathcal{L}}{\nu_0}, \tag{11}$$

and the Weissenberg number ($Wi_{\mathcal{L}}$),

$$Wi_{\mathcal{L}} = \frac{\lambda U_\infty}{\mathcal{L}}, \tag{12}$$

where U_∞ is the free stream velocity and $\mathcal{L}$ is the length of the flat plate. The local coordinate x will also be used later as a characteristic length scale.

In the 2D planar boundary layer flow continuity is immediately enforced by the introduction of the stream function ψ

$$u = \frac{\partial\psi}{\partial y}, \quad v = -\frac{\partial\psi}{\partial x}, \tag{13}$$

which, upon substitution into the x-momentum balance and considering steady state flow conditions, leads to the following simpli-

fied equation:

$$\left(\frac{\partial\psi}{\partial y}\right)\left(\frac{\partial^2\psi}{\partial x\partial y}\right)-\left(\frac{\partial\psi}{\partial x}\right)\left(\frac{\partial^2\psi}{\partial y^2}\right) = (1-\beta_p)\upsilon_0\left(\frac{\partial^3\psi}{\partial y^3}\right)+\frac{\beta_p\upsilon_0}{\lambda}\frac{\partial\left(f(C_{kk})C_{xy}\right)}{\partial y}, \tag{14}$$

where the solvent and polymer shear stresses have been substituted by their definitions in Eqs. (4) and (6). The variations of C_{xy} and $f(C_{kk})$ from the conformation tensor equation are required to get a closed form solution.

The validity of the boundary layer approximation in the momentum equation requires large Reynolds number flows. Additionally, since both shear stresses were kept in the equation, there is no restriction on the Weissenberg number, as discussed in Parvar et al. [37].

An order of magnitude analysis of the evolution equation for the conformation tensor was also carried out by Parvar et al. [37] for this flow. As discussed there in detail, by considering the velocities through the stream function, and assuming $\partial\psi/\partial x << \partial\psi/\partial y$ and further assuming the Weissenberg number to be sufficiently low that the normal components of the conformation tensor are much larger than the shear components (at rest $C_{xx}=C_{yy}=C_{zz}\cong 1$ and $C_{ij\ (i\neq j)}$=0 (to ensure null deviatoric stress)), the simplified evolution equations for the components of the conformation tensor for steady-state flow become

$$-2\lambda C_{xx}\frac{\partial^2\psi}{\partial x\partial y}-2\lambda C_{xy}\frac{\partial^2\psi}{\partial y^2}+f(C_{kk})C_{xx}=f_e(L), \tag{15}$$

$$2\lambda C_{yy}\frac{\partial^2\psi}{\partial x\partial y}+f(C_{kk})C_{yy}=f_e(L), \tag{16}$$

$$f(C_{kk})C_{zz}=f_e(L), \tag{17}$$

$$-\lambda C_{yy}\frac{\partial^2\psi}{\partial y^2}+f(C_{kk})C_{xy}=0. \tag{18}$$

So, a restriction on the Weissenberg number is imposed by the constitutive equation through the quality of its predictions of C_{ij}, as discussed later. Further manipulation provides the following algebraic equations for the components of C_{ij} which depends on the flow characteristics via the stream function, other C_{ij} components and the trace of the conformation tensor (C_{kk}) via the Peterlin function, which is obtained from Eq. (7-c).

$$C_{xx}=\frac{f_e(L)+2\lambda C_{xy}\frac{\partial^2\psi}{\partial y^2}}{\left(f(C_{kk})-2\lambda\frac{\partial^2\psi}{\partial x\partial y}\right)} = f_e(L)\frac{f(C_{kk})\left(2\lambda\frac{\partial^2\psi}{\partial x\partial y}+f(C_{kk})\right)+2\lambda^2\left(\frac{\partial^2\psi}{\partial y^2}\right)^2}{f(C_{kk})\left(f(C_{kk})^2-\left(2\lambda\frac{\partial^2\psi}{\partial x\partial y}\right)^2\right)}, \tag{19}$$

$$C_{yy}=\frac{f_e(L)}{\left(2\lambda\frac{\partial^2\psi}{\partial x\partial y}+f(C_{kk})\right)}, \tag{20}$$

$$C_{zz}=\frac{f_e(L)}{f(C_{kk})}, \tag{21}$$

$$C_{xy}=\frac{\lambda C_{yy}\frac{\partial^2\psi}{\partial y^2}}{f(C_{kk})}=\frac{\lambda f_e(L)\frac{\partial^2\psi}{\partial y^2}}{f(C_{kk})\left(f(C_{kk})+2\lambda\frac{\partial^2\psi}{\partial x\partial y}\right)}. \tag{22}$$

Summing the three normal components gives the trace of conformation tensor C_{kk}

$$C_{kk}=f_e(L)\frac{3f(C_{kk})^2+2\lambda^2\left(\frac{\partial^2\psi}{\partial y^2}\right)^2-4\lambda^2\left(\frac{\partial^2\psi}{\partial x\partial y}\right)^2}{f(C_{kk})\left(f(C_{kk})^2-4\lambda^2\left(\frac{\partial^2\psi}{\partial x\partial y}\right)^2\right)}. \tag{23}$$

For a steady state thermal boundary layer flow $\partial^2T/\partial x^2 << \partial^2T/\partial y^2$ as in a Newtonian boundary layer flow. In addition, since $\tau_{xx}\frac{\partial u}{\partial x} << \tau_{xy}\frac{\partial u}{\partial y}$ and further assuming a constant thermal conductivity fluid, the boundary layer approximations applied to the energy Eq. (9) reduce it to

$$\left(u\frac{\partial T}{\partial x}+v\frac{\partial T}{\partial y}\right)=\frac{k}{\rho c_p}\left(\frac{\partial^2T}{\partial y^2}\right)+\frac{1}{\rho c_p}\left(\tau_{xy}\frac{\partial u}{\partial y}\right). \tag{24}$$

In reality fluid properties may depend on temperature, however the temperature variation is postulated to be small in the present study, therefore thermodynamic and transport fluid properties such as k and c_p are assumed to be constant. Here it is also assumed that the effect of the viscous dissipation term is non-negligible since polymer-based fluids are often reasonably viscous.

Expressing the total shear stress on the basis of solvent and polymer quantities, and introducing the stream function and the expression for C_{xy}, we arrive at the following form of the energy equation

$$\left(\frac{\partial\psi}{\partial y}\frac{\partial T}{\partial x}-\frac{\partial\psi}{\partial x}\frac{\partial T}{\partial y}\right)=\alpha\left(\frac{\partial^2T}{\partial y^2}\right)+\frac{\upsilon_0}{c_p}\left(\frac{\partial^2\psi}{\partial y^2}\right)^2 \times\left(\frac{(1-\beta_p)f(C_{kk})+2\lambda(1-\beta_p)\frac{\partial^2\psi}{\partial x\partial y}+\beta_p f_e(L)}{\left(f(C_{kk})+2\lambda\frac{\partial^2\psi}{\partial x\partial y}\right)}\right) \tag{25}$$

where α is the fluid thermal diffusivity ($\alpha=k/(\rho c_p)$).

3.2. Transformed governing equations

Inspired by the self-similarity of the corresponding approximate solution for Newtonian fluids [38,39], which only depends on the similarity variable (η), the above governing equations can be further manipulated to facilitate their numerical solution as originally done by Olangunju [18,33]. However, as discussed in detail there and in Parvar et al. [35–37], the FENE-P solution depends not only on η but also on x. Hence the similarity variables to be used are η and function $G(\eta,x)$ defined as

$$\eta=\sqrt{\frac{U_\infty}{2\nu_0}}\frac{y}{x^{1/2}},\ G(\eta,x)=\frac{\psi}{\sqrt{2U_\infty\nu_0}x^{1/2}}. \tag{26}$$

The flow streamwise and normal velocities are obtained from their definitions, as

$$u=U_\infty G'(\eta,x), \tag{27}$$

$$v=\sqrt{\frac{\nu_0U_\infty}{2x}}\left(\eta G'(\eta,x)-G(\eta,x)\right), \tag{28}$$

where the derivatives of $G(\eta,x)$ with respect to η are shown with primes. Even though $G(\eta,x)$ depends on both η and x, to avoid an excessively complicated solution and since its streamwise derivative is smaller than its cross-stream derivative, the former is here assumed negligible ($\frac{\partial G(\eta,x)}{\partial x}\approx 0$), to allow a simpler differential equation that is more easily solved numerically, as previously done by Olagunju [18,33] and Parvar et al. [35–37,55].

Regarding the constitutive equation, the transformed Peterlin function becomes also dependent on both η and x when using the

similarity variables, as explained by Olagunju [18,33] and Parvar et al. [35–37,55], and is here redefined as

$$K(\eta, x) = f(C_{kk}) \tag{29}$$

in order to emphasize the local nature of the solution. Using any of the Peterlin functions in Eq. (7-c) leads to the following third order algebraic equation for $K(\eta, x)$

$$K^3 + C_0 K^2 - {Wi_x}^2 \left(\eta G''\right)^2 K + C_1 G''^2 + C_2 \left(\eta G''\right)^2 = 0 \tag{30}$$

with dimensionless coefficients

$$C_0 = \left(\frac{3I - 3f_e(L) - L^2}{L^2}\right),$$

$$C_1 = -\frac{\lambda^2 f_e(L) {U_\infty}^3}{\nu_0 L^2} x^{-1} = -\frac{f_e(L) Re_x {Wi_x}^2}{L^2},$$

$$C_2 = \frac{\lambda^2 \left(L^2 + f_e(L) - 3I\right) {U_\infty}^2}{L^2} x^{-2} = \frac{\left(L^2 + f_e(L) - 3I\right) {Wi_x}^2}{L^2}. \tag{31}$$

where $I = 1$ for the Peterlin function of Eq. (7-c), and $I = 0$ for (7-a) and (7-b).

With further mathematical manipulation (see [37] for details), the following final form of the momentum equation is obtained

$$G''' = -\frac{GG'' + \beta_p f_e(L) G'' \frac{\left(Wi_x C_4 G'' + 2C_3 \left(C_2 - Wi_x^2 K\right)\right)}{\left(K - Wi_x \eta G''\right)^2 C_4}}{\left((1-\beta_p) + \beta_p f_e(L) \frac{\left(C_4 K + 2G''^2 \left(C_1 + \eta^2 \left(C_2 - Wi_x^2 K\right)\right)\right)}{\left(K - Wi_x \eta G''\right)^2 C_4}\right)} \tag{32}$$

with

$$C_3 = \eta G''^2, C_4 = \left(3K^2 + 2C_0 K - Wi_x^2 \left(\eta G''\right)^2\right) \tag{33}$$

The numerical solution of Eqs. (30) and (32) is explained in the next Section.

Regarding the heat transfer equation, its normalization depends on the imposed wall thermal boundary condition. Here we study two popular boundary conditions in heat transfer, the constant wall temperature (T_w) and constant wall heat flux (q_w), leading to different definitions for the dimensionless temperature. For the former case, the constant wall temperature case, the dimensionless temperature is defined as

$$\theta(\eta) = \frac{T(x,y) - T_\infty}{T_w - T_\infty}, \tag{34}$$

where T_∞ is the temperature of the free stream flow over the thin motionless semi-infinite flat plate kept at a constant temperature (T_w). Substituting Eqs. (26)–(29) and Eq. (34) into Eq. (25) the final transformed energy equation becomes

$$\theta'' + PrG\theta' + Br\left(\frac{(1-\beta_p)K - (1-\beta_p) Wi_x \eta G'' + \beta_p f_e(L)}{(K - Wi_x \eta G'')}\right) G''^2 = 0 \tag{35}$$

where Pr is the Prandtl number ($Pr = \upsilon_0/\alpha$) and Br is the global Brinkman number defined as

$$Br = \frac{Pr {U_\infty}^2}{c_p (T_w - T_\infty)} \tag{36}$$

For the latter case of the thermal flow problem with a constant wall heat flux (q_w) the dimensionless temperature is defined differently as

$$\theta(\eta) = \frac{T(x,y) - T_\infty}{\Delta T(x)} = \frac{T(x,y) - T_\infty}{\frac{q_w}{k}\sqrt{\frac{2\upsilon_0 x}{U_\infty}}} = \frac{T(x,y) - T_\infty}{\frac{q_w x \sqrt{2}}{k\sqrt{Re_x}}} \tag{37}$$

and by substituting Eqs. (26)–(29) and Eq. (37) into Eq. (25) the final transformed energy equation becomes

$$\theta'' - Pr\left(\theta G' - G\theta'\right) + Br_x \left(\frac{(1-\beta_p)K - (1-\beta_p) Wi_x \eta G'' + \beta_p f_e(L)}{(K - Wi_x \eta G'')}\right) G''^2 = 0 \tag{38}$$

which also depends on a local Brinkman number based on the local temperature difference ($\Delta T(x)$) and here defined as

$$Br_x = \frac{Pr {U_\infty}^2}{c_p \Delta T(x)} = \frac{Pr {U_\infty}^2}{c_p \frac{\sqrt{2} q_w x}{k\sqrt{Re_x}}} = \frac{Pr {U_\infty}^2 k \sqrt{Re_x}}{c_p \sqrt{2} q_w x} \tag{39}$$

To summarize, for the same flow condition (steady boundary layer flow over a flat plate with zero pressure gradient of viscoelastic FENE-P fluids) we are solving two different and independent thermal cases, the constant wall temperature case Eqs. (34)–(36) and the constant wall heat flux case Eqs. (37)–(39), for both problems always considering constant thermal fluid properties. Each thermal case has its own definition of the dimensionless temperature and Brinkman number leading to a specific form of the simplified thermal energy equation, which are more complex than for the corresponding Newtonian fluid cases (cf. [38,39,56]) on account of the fluid viscoelasticity. As mentioned in the introduction, a more accurate version of the simplified constitutive equation is used in this work than originally by Olagunju [18,33] leading to improved predictions of the stress tensor and this has implications both on the velocity profile, but especially upon the stress work term in the thermal energy equation, which differs from that in Olagunju [18].

4. Numerical solution of the governing equations

The simplified governing equations for the dynamic problem are a third-order differential equation on $G(\eta, x)$ and an algebraic cubic equation for $K(\eta, x)$, the same equations as in Parvar et al. [37]. Consequently, they are solved numerically following the same procedure namely, the third-order differential equation is converted to a system of first-order differential equations by considering the following transformations, $G_1 = \frac{\partial^2 G}{\partial \eta^2}$, $G_2 = \frac{\partial G}{\partial \eta}$ and $G_3 = G(x, \eta)$, alternatively written as

$$\frac{dG_1}{d\eta} = G''', \tag{40}$$

$$\frac{dG_2}{d\eta} = G_1, \tag{41}$$

$$\frac{dG_3}{d\eta} = G_2 \tag{42}$$

since $\partial G/\partial x = 0$. First, the Cardan-Tartaglia formula [57,58] provides the real solution of the cubic algebraic equation. This solution must be physically correct, i.e., the normal components of the conformation tensor must be positive, and its trace should lie between 3 (the value at rest) and the square of the maximum dumbbell extensibility (L^2). Then, the system of differential equations is numerically solved with a fourth-order Runge–Kutta procedure coupled with a shooting method to apply the boundary conditions [59,60].

The boundary conditions for the momentum equation of laminar flat plate boundary layer flow are [38,39]:

$$G'(x, \infty) \to 1, G(x, 0) = G'(x, 0) = 0. \tag{43}$$

For the thermal problem, the second-order differential equations on $\theta(x,\eta)$ (each thermal problem has its own equation) are also solved with the fourth order Runge-Kutta method and the

same shooting method is used to apply the following two sets of thermal boundary conditions:

(i) for the constant wall temperature

$$\theta(x,0)=1,\ \ \theta(x,\infty)=0; \tag{44}$$

(ii) for the constant wall heat flux

$$\theta'(x,0)=-1,\ \ \theta(x,\infty)=0. \tag{45}$$

5. Results and discussion

5.1. Verification: Newtonian fluids

The governing equations for the boundary layer flow of the viscoelastic fluid reduce to those for a Newtonian flat plate flow [38,39] for $\beta_p = 0$ and this was used to verify the dynamic solution in Parvar et al. [37], therefore only the energy equation is verified next. In this work, similar to Parvar et al. [37] in terms of dynamics, the length of the computational domain was set to $\eta = 10$ following White [38], who showed that at $\eta = 10$ the flow characteristics approach the boundary conditions at infinity in his asymptotic analysis. The number of grid points used in our simulations was 2000 leading to a cell size $\Delta\eta = 0.005$, and the corresponding numerical uncertainty is estimated to be below 0.001%. This was assessed in a comparison of G and θ obtained in our mesh with the corresponding values in a simulation with 4000 grids points and cell size $\Delta\eta = 0.0025$, where the relative difference was of about 1×10^{-6}.

Fig. 2 (a) shows excellent agreement in the comparisons between the numerical values of dimensionless temperature from the current solution and the literature for the constant wall temperature case and for Prandtl numbers (Pr) of interest in the context of viscoelastic liquids [38].

The corresponding Nusselt number (Nu) variation, is defined as

$$Nu_x = \left(\frac{h_x x}{k}\right), \tag{46}$$

where h_x is the local convection coefficient plotted in Fig. 2 (b). The local convection coefficient is defined by Newton's cooling law, $h_x = (\frac{q_w}{T_w - T_\infty})$, and the wall heat flux is given by Fourier's law at the wall, $q_w = -k(\frac{\partial T}{\partial y})_{y=0}$. Further manipulation provides the following expression for the local Nusselt number of the constant wall temperature case

$$Nu_x = \left(-\theta'(0)\right)\sqrt{\frac{Re_x}{2}}. \tag{47}$$

The comparisons in Fig. 2 (b) include the effect of Prandtl number Pr and show excellent agreement with the literature [39].

For the constant wall heat flux (q_w) the wall temperature varies with x and is part of the solution. Manipulation involving Newton's law of cooling and Fourier's law at the wall leads to the local Nusselt number of

$$Nu_x = \frac{1}{\theta(0)}\sqrt{\frac{Re_x}{2}} \tag{48}$$

The comparison with the literature is again excellent, but is not shown for conciseness. As expected, for the Newtonian fluid case, the final solution is independent of the location (x).

5.2. FENE-P fluids

In this section, we present results for the thermal solutions for the FENE-P fluid defined with the third set of Peterlin functions, Eq. (7-c).

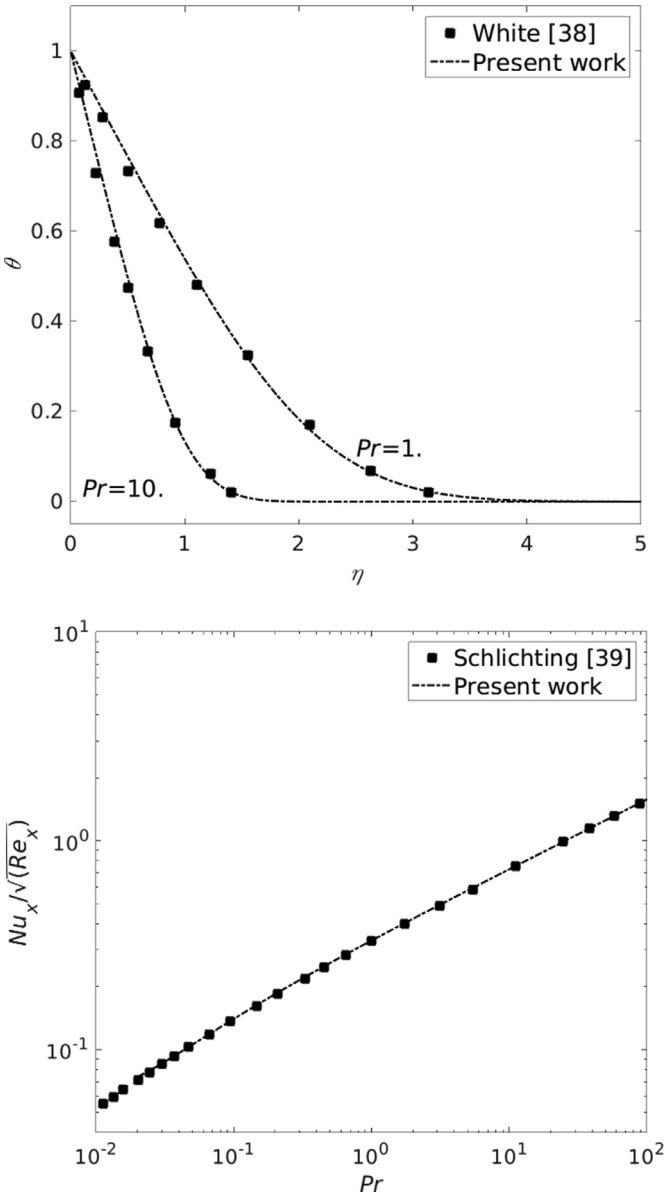

Fig. 2. Characteristics of the thermal laminar boundary layer flow of Newtonian fluid for a constant wall temperature: a) Variation of θ with Pr; b) Variation of $\frac{Nu_x}{\sqrt{Re_x}}$ with Pr. Lines represent data from the present work and symbols represent data from the literature [38,39].

5.2.1. Validation: FENE-P fluids

We start with a comparison between the approximate local solution and the results of a numerical solution of the full set of governing equations using the RheoFoam toolbox of OpenFoam [40,41], which is based on a finite volume method. The full numerical solution relies on the high-order resolution scheme CUBISTA [61] for the advective terms of the momentum, energy and conformation equations and central differences for the diffusive terms. The computational domain had a length $1.2\mathcal{L}$, divided into two blocks: block I upstream the plate leading edge was $0.2\mathcal{L}$ long, block II along the plate had a length of $\mathcal{L}$ and the width of both blocks was larger and set at $2.0\mathcal{L}$. In each block the non-uniform computational grid had $N_x \times N_y \times N_z$ cells in the x, y, z directions, respectively as given in Table 1 together with the expansion/contraction factors $f_x = \Delta_x^{i+1}/\Delta_x^i$ and $f_y = \Delta_y^{i+1}/\Delta_y^i$ and ratios of mesh size over boundary layer thickness at some locations. As reported by Parvar [37] the mesh with $N_x \times N_y$ =200×600 cells in

Table 1
Characteristics of the meshes used in the RheoFoam calculations for verification. The values of Δx and Δy listed pertain to the cells nearest the wall.

Block	N_x	N_y	N_z	f_x	f_y	$\frac{\Delta x_{x=0}}{\delta_{ux=\mathcal{L}}}$, $\frac{\Delta y_{x=0}}{\delta_{ux=\mathcal{L}}}$	$\frac{\Delta x_{x=\mathcal{L}}}{\delta_{ux=\mathcal{L}}}$
I	20	600	1	0.886	1.0088	-	-
II	200	600	1	1.0116	1.0088	0.0443,0.0051	0.443

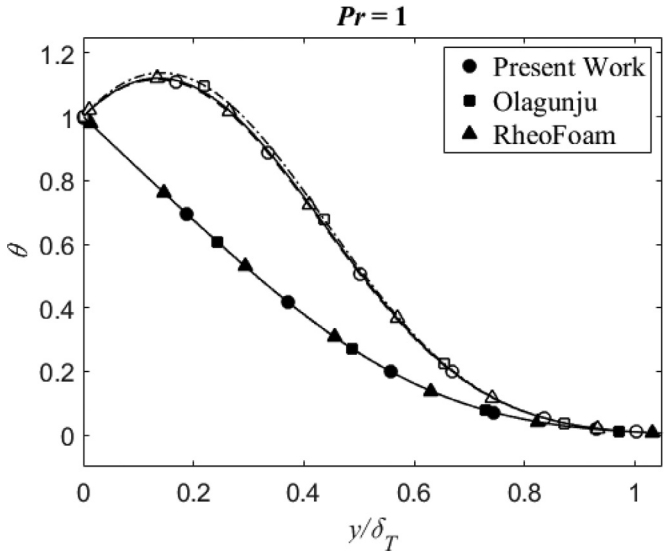

Fig. 3. Normalized transverse temperature profiles at $\frac{x}{\mathcal{L}} = 0.2$ for $\beta_p = 0.1$, $L^2 = 900$, Re_x=2×10^4 and Wi_x=1.0. Comparison between the present work (circles), Olagunju (squares), and RheoFoam (triangles) for the constant wall temperature problem with Pr=1 and Br=0 (closed symbols), Br=4 (open symbols).

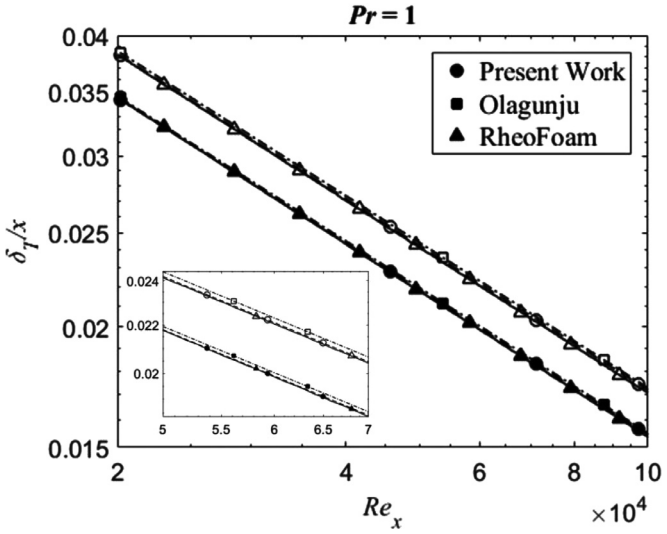

Fig. 4. Streamwise variation of the normalized thermal boundary layer thickness (δ_T/x) for $\beta_p = 0.1$, $L^2 = 900$, $Re_{\mathcal{L}}$=10×10^4 and $Wi_{\mathcal{L}}$= 0.2. Comparison between the present work (circles), Olagunju (squares), and RheoFoam (triangles) for the constant wall temperature problem with Pr=1 and Br=0 (closed symbols), Br=4 (open symbols). The inset plots profiles for $5\times10^4 \le Re_x \le 7\times10^4$.

the second block was selected after an assessment of mesh independence using four grids 50 × 100, 100 × 300, 200 × 600, and 400 × 1200. The discrepancy between the results of the normalized transverse u/U_∞velocity profiles of grids 200 × 600 and 400 × 1200 is below 0.05% (the number of cells in block I and the expansion/contraction factors were consistently changed when refining/ coarsening grids).

A uniform velocity was imposed at the inlet boundary and a zero gradient condition was set for all quantities at the outlet boundary, while no slip conditions were considered at the flat wall. At the boundary immediately upstream the wall, within block I, symmetry conditions were set. Finally, for the far-field boundary condition, i.e. the boundary opposite the wall, free stream velocity conditions were imposed, both in blocks I and II.

The simulations were carried out for the Peterlin function of Eq. (7-c) with $\beta_p = 0.1$ and $L^2 = 900$ and the results shown pertain to $x/\mathcal{L} = 0.2$, where the local Reynolds and Weissenberg numbers (Re_x and Wi_x) defined as per Eqs. (11) and (12), are Re_x= 2 × 10^4 and Wi_x= 1.0, respectively. Fig. 3 compares the normalized transverse temperature profiles of the constant wall temperature problem with Pr=1 and shows the excellent agreement between the current solution and RheoFoam simulations in the absence (Br=0) and with viscous dissipation effects (Br=4). The comparison with Olagunju's work shows some discrepancy which tends to increase with viscous dissipation (Br=4) especially in regions where such effects are stronger, as near the wall, leading to 3% relative error compared with Rheofoam results. For higher elasticity (not shown for conciseness), these differences will tend to increase.

Figs. 4 and 5 compare the streamwise variations of the normalized thermal boundary layer thickness (δ_T/x) and of the Nusselt number (Nu_x), respectively obtained from the present study and from RheoFoam for the same cases ($\beta_p = 0.1$, $L^2 = 900$, $Re_{\mathcal{L}}$=10^5 and $Wi_{\mathcal{L}}$= 0.2, Pr=1 for Br=0 and 4). The comparisons of the present work with RheoFoam are good for these cases in which the wall temperature is higher than the free stream temperature. As shown, the present semi-analytical results can predict the normalized thermal boundary layer thickness more accurately than Olagunju's, but this difference is small in terms of this physical quantity, maximum 1% relative error for the presented results, tending to increase with viscous dissipation and flow elasticity. For the case with Br=4 viscous dissipation is sufficiently strong to make the fluid near the wall warmer than the wall itself, therefore this thin near wall layer of fluid is cooled simultaneously by the wall and by the free stream. Hence, and in relation to the negligible viscous dissipation flow, there is an inversion in the direction of the wall heat flux from positive to negative (cf. coordinate system in Fig. 1) and consequently the Nusselt number definition leads to negative values of Nu_x (Fig. 5 (b)). In the absence of viscous dissipation (cf. Fig. 5 (a)), the disagreement in Nu_x between Olagunju's work on one side and RheoFoam and the present semi-analytical solution on the other, is slight but it significantly increases with the magnitude of the Brinkman number, leading to maximum 10% relative error for Br = 4, as shown in Fig. 5 (b).

Before proceeding, it is important to discuss the characteristic length scale used to define the Reynolds and Weissenberg numbers. As explained by Parvar et al. [37] the boundary layer thickness (δ_u) is a more adequate characteristic length scale than x, but δ_u is part of the solution making it more difficult to quantify *a-priori*, hence the use of Re_x and Wi_x instead of Re_{δ_u} and Wi_{δ_u}. Since the numerical values of Wi_x are lower than the corresponding local values of Wi_{δ_u} one may be misled into thinking that the limit of validity of the approximate solution corresponds to conditions of low elasticity flow, which is not the case. Indeed, for an appropriate assessment of the magnitudes of Wi_x and Wi_{δ_u} Fig. 6 plots the variations of both quantities for the present flows showing that Wi_{δ_u} is at least one order of magnitude higher than Wi_x: for the cases in Fig. 6 where $0.2 < Wi_x < 1.0$, one gets $13 < Wi_{\delta_u} < 29$ hence corresponding to significant elastic effects.

The previous work [37] observed that above Wi_x=0.2 to 0.3 the semi-analytical solution starts to be unable to describe the complex variations of the conformation tensor components within the boundary layer, but nevertheless it is still possible to predict the dynamic boundary layer thickness, the velocity profiles and

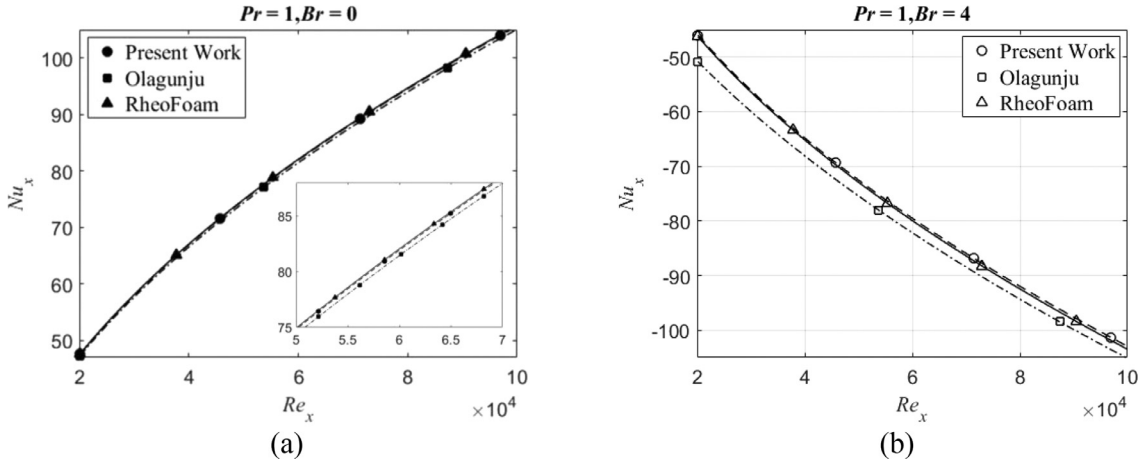

Fig. 5. Comparison between streamwise variation of the Nusselt number (Nu_x) for $\beta_p = 0.1$, $L^2 = 900$, $Re_{\mathcal{L}}$=10^5 and $Wi_{\mathcal{L}}$= 0.2 from the present work (circles), Olagunju (squares), and RheoFoam (triangles) for the constant wall temperature problem with: (a) Pr=1 and Br=0 (closed symbols), (b) Pr=1 and Br=4 (open symbols). The inset in (a) plots profiles for $5 \times 10^4 \leq Re_x \leq 7 \times 10^4$.

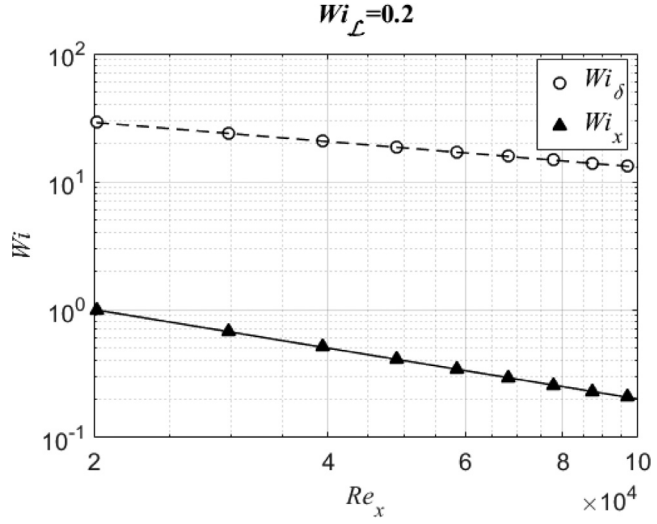

Fig. 6. Streamwise variation of Wi_x (triangles and solid lines) and local Wi_δ (circles and dashed line) for $\beta_p = 0.1$, $L^2 = 900$. and $Re_{\mathcal{L}}$ =10^5. Lines are a guide to the eye.

the friction coefficient to within 5% for Wi_x of up to 5. Similarly, for the thermal boundary layer, the semi-analytical solution is in good agreement with the RheoFoam simulations in terms of dimensionless temperature profile, thermal boundary layer thickness and Nusselt number for $Wi_x \leq 5$.

Finally, it is noteworthy to compare the computational cost of the present approximate thermal solutions and of the corresponding RheoFoam simulations. The latter were carried out by a computer equipped with an Intel Xeon E5 processor with 12 MB L3 cache and Turbo Boost up to 3.9 GHz, with parallel processing using its 6 computer cores, which took approximately 5.0 hours to complete. In contrast, the computational cost of the semi-analytical solutions was about one second using a single core in the same machine.

5.2.2. Thermal boundary layer flow of FENE-P fluids with constant wall temperature

Without the presence of viscous dissipation the normalized thermal behavior is the same regardless the fluid is heating or cooling, but since the current solution includes the stress work contribution this section deals first with wall heating followed by wall cooling (designation based on the case with viscous dissipation). In both cases results are compared with data without viscous dissipation ($Br = 0$).

(a) $T_w > T_\infty$ (wall heating)

Transverse profiles of normalized temperature (θ) at two different locations are shown in Fig. 7 (a),(b). By using the dimensionless transverse coordinate η, quasi-unique profiles are obtained at low elasticity levels for each value of Br, which coincide with the corresponding Newtonian profiles. However, by enhancing the elasticity level, small deviations from the low elasticity asymptote are observed, associated with the simultaneous dependence of the solution on x which is proportional to flow elasticity.

Since the wall is warmer than the free stream fluid, viscous dissipation corresponds to a positive Brinkman number ($Br > 0$) which increases the dimensionless temperature. For weak viscous dissipation the maximum temperature is still at the flat plate, but the fluid near the wall becomes warmer than for $Br = 0$. At a sufficiently high value of Br a local peak temperature within the fluid exceeds the wall temperature leading to an inversion of the wall heat flux and a thin layer of near wall warm fluid is now simultaneously cooled by the wall and by the free stream. The critical value of Br marking this transition (Br_c) corresponds to a zero-wall heat flux and, as shown in Fig. 7-(a) for a Newtonian fluid at $Pr = 1$ we have Br_c= 2. Br_c increases with Pr, so that at $Pr = 10$ $Br_c = 6.79$. Increasing elasticity levels slightly increase the value of Br_c, so that at the maximum elasticity level in Fig. 7 (a) and (b) ($Wi_{\mathcal{L}}$=0.1, $\beta_p = 0.5$, L=30) the values of the critical Br number are 2.1 and 7.05 for $Pr = 1$ and 10, representing increases of 4.5% and 3.5% relative to the corresponding Newtonian values, respectively. As Br further increases beyond Br_c the peak temperature progressively rises and its location moves away from the wall as the amount of internally heated fluid grows. The deviation of the dimensionless temperature for the highest elasticity condition from the corresponding Newtonian curve is 6% pertaining to $Br_{\mathcal{L}} = 40$. In addition, as elasticity is increased in the presence of viscous dissipation the location of maximum θ slightly moves toward the wall.

Fig. 8 shows the streamwise variation of the compensated local Nusselt number ($Nu_x/\sqrt{Re_x}$) displayed as a function of flow and fluid characteristics. As expected, this quantity is constant for flows with vanishing elasticity, but as $Wi_{\mathcal{L}}$ and β_p increase and L decreases, the ratio $Nu_x/\sqrt{Re_x}$ increases and varies quasi-linearly along the plate (the ordinate is zoomed), but always tending to the Newtonian value as Re_x increases because simultaneously Wi_x decreases on going downstream. It is also observed that as viscous

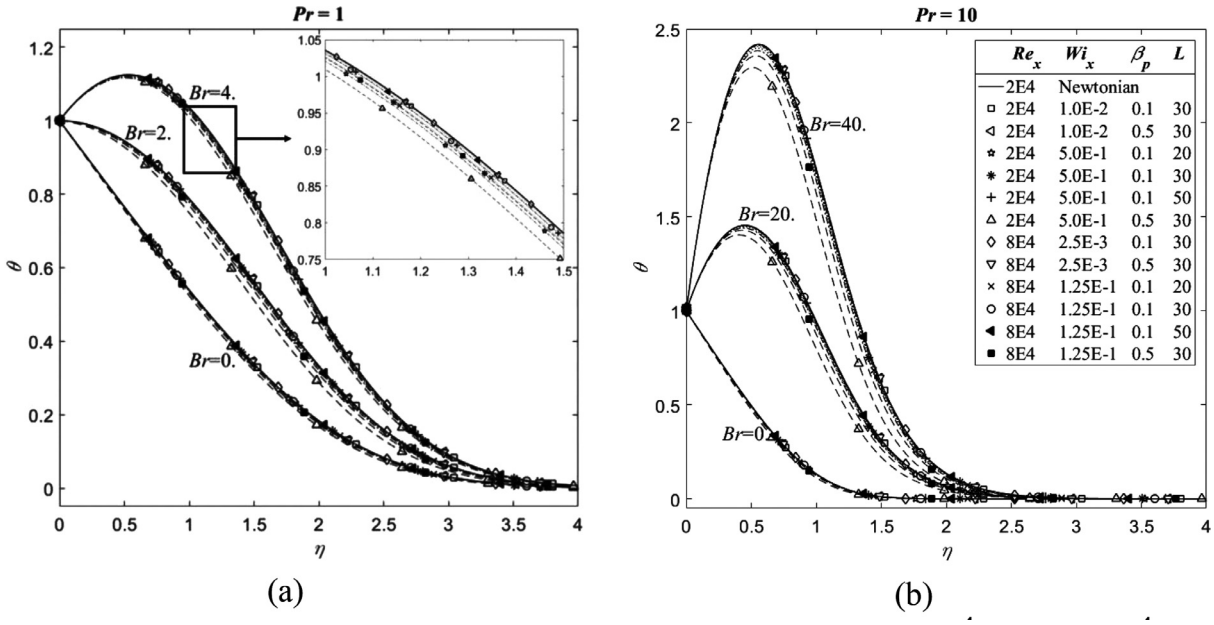

Fig. 7. Normalized transverse temperature profiles at $Re_x = 2 \times 10^4$ and 8×10^4 as a function of local Reynolds and Weissenberg numbers, viscosity ratio and dumbbell extensibility for constant wall temperature with (a) Pr=1, (b) $Pr = 10$. The inset plots profiles for $1 \leq \eta \leq 1.5$.

dissipation increases, the dependence of the ratio $Nu_x/\sqrt{Re_x}$ on Re_x weakens. For these cases, the compensated Nusselt number can be increased by elasticity by up to 6%.

The interaction between viscous dissipation and elasticity depends on whether Br is below or above Br_c, as shown in Fig. 8: for $Br \leq Br_c$ enhancing elastic effects increases Nu_x whereas for $Br > Br_c$ increasing flow elasticity reduces the absolute value of Nu_x, i.e, not only there is a reversal in the heat flux direction but its magnitude also decreases. We also see that these variations increase with Pr but in inverse proportion to Br, meaning that by increasing Br beyond its critical number Br_c, increasing elasticity decreases the magnitude of Nu_x.

The streamwise variation of the thermal boundary layer thickness (δ_T/x) is plotted in Fig. 9 as a function of $Wi_{\mathcal{L}}$, β_p and L, respectively. At low Weissenberg numbers δ_T/x collapse to the Newtonian flow curve, but by increasing $Wi_{\mathcal{L}}$, β_p, or decreasing L, at the same value of Br, the boundary layer thickness decreases (under the conditions of this analysis δ_u does not depend on Br). Nevertheless, by increasing Br more heat is generated inside the thermal boundary layer, hence thickening it. Here, the maximum reduction of the thermal boundary layer thickness by elasticity is 4%.

(b) $T_w < T_\infty$ (wall cooling)

In this section, the effects of elasticity and viscous dissipation are studied for a flow over a cold flat plate surface. In all cases the fluid will be warmer than the wall and there will be cooling at the surface.

Considering the temperature normalization of Eq. (34), the dimensionless temperature will vary from 1 at the wall to 0 outside the thermal boundary layer, as shown in the plots of Fig. 10. For this thermal condition, viscous dissipation means a negative Brinkman number and as Br progressively increases in magnitude the profiles of dimensionless temperature shift downward (become more negative) as shown in Fig. 10 (a) and (b). For $Pr = 1$ in the range of $-2 < Br < 0$ for Newtonian fluids, the loci of maximum and minimum dimensionless temperatures do not change, but when the magnitude of Br exceeds a critical value, $Br_c = -2$ for Newtonian fluids with $Pr = 1$, viscous dissipation becomes so intense near the wall region that a local dimensionless temperature minimum develops inside the thermal boundary layer ($\theta < 0$) and progressively moves towards the plate as Br becomes increasingly negative. This corresponds to a dimensional temperature inside the thermal boundary layer exceeding the free-stream temperature, therefore there is an inversion in the heat flux far from the wall, i.e. this near wall fluid layer is simultaneously cooled by the wall and by the free stream flow. This critical Brinkman number decreases significantly in magnitude with Pr so that, for example, for Newtonian fluids with $Pr = 10$, $Br_c \cong -0.1$. Regarding the effect of flow elasticity, i.e., increasing $Wi_{\mathcal{L}}$, β_p, or decreasing L, a slight weakening of the effects of viscous dissipation is seen, and moves the location of the minimum temperature slightly towards the wall. We also notice that for the highest viscous dissipation tested ($Br_{\mathcal{L}} = 40$), the elasticity reduces by 10% the magnitude of dimensionless temperature.

Fig. 11 (a),(b) show the corresponding effects of Pr, elasticity and viscous dissipation on the Nusselt number, bearing in mind that for $Br = 0$ the behavior is independent of whether the wall is cooling or heating. As displayed, increasing elasticity levels and the magnitude of the negative Br enhance heat transfer, regardless of Pr and of whether Br is below or above Br_c, which contrasts with findings for the fluid heating case. Here, the maximum deviation from the Newtonian curves is 2%

Fig. 12 (a),(b) shows the effect of elasticity and viscous dissipation on thermal boundary layer thickness. As defined in Section 2 the threshold for the end of the thermal boundary layer is the location where $|\theta(\eta)| = 0.01$. When viscous dissipation is weak θ varies monotonically and there is a single location which satisfies the criterion. In contrast, for $Br > Br_c$ the temperature θ changes sign and consequently there are now three locations which match the threshold value as shown in Fig. 10 (a) and (b). In this circumstance the location which is consistent with the physical concept of thermal boundary layer thickness is the one closest to the free stream thermal condition.

Therefore, in this set-up and according to the strength of viscous dissipation we observed two different behaviors for variation of thermal boundary layer thickness. At subcritical Brinkman numbers ($-2 < Br < 0$) and for $Pr = 1$ enhancing elasticity increases the thermal boundary layer thickness. For $Pr \geq 1$ there is synergy

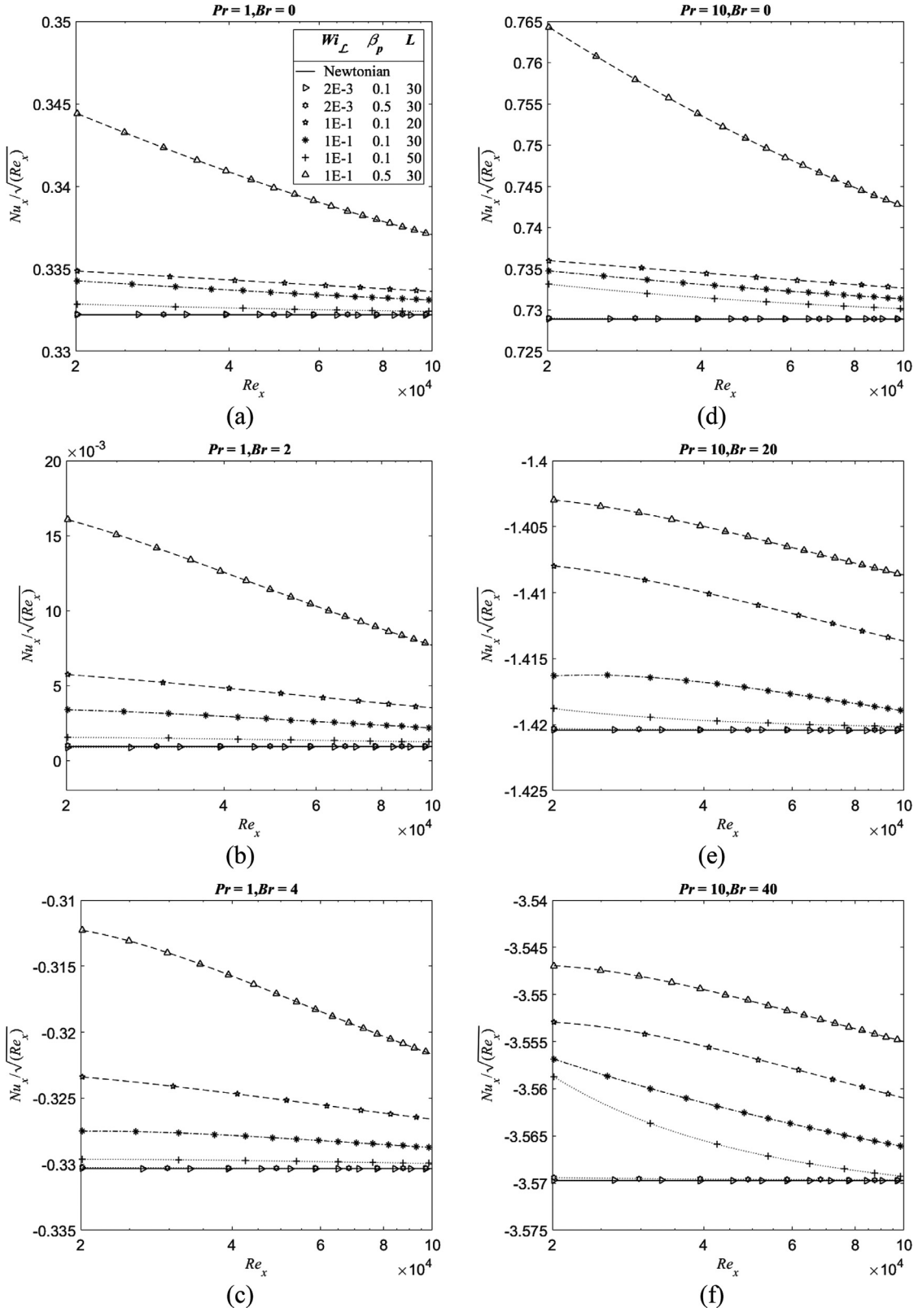

Fig. 8. Streamwise variation of the compensated Nusselt number ($Nu_x/\sqrt{Re_x}$) under various flow conditions for constant wall temperature with (a)-(c) Pr=1, and (d)-(f) Pr = 10.

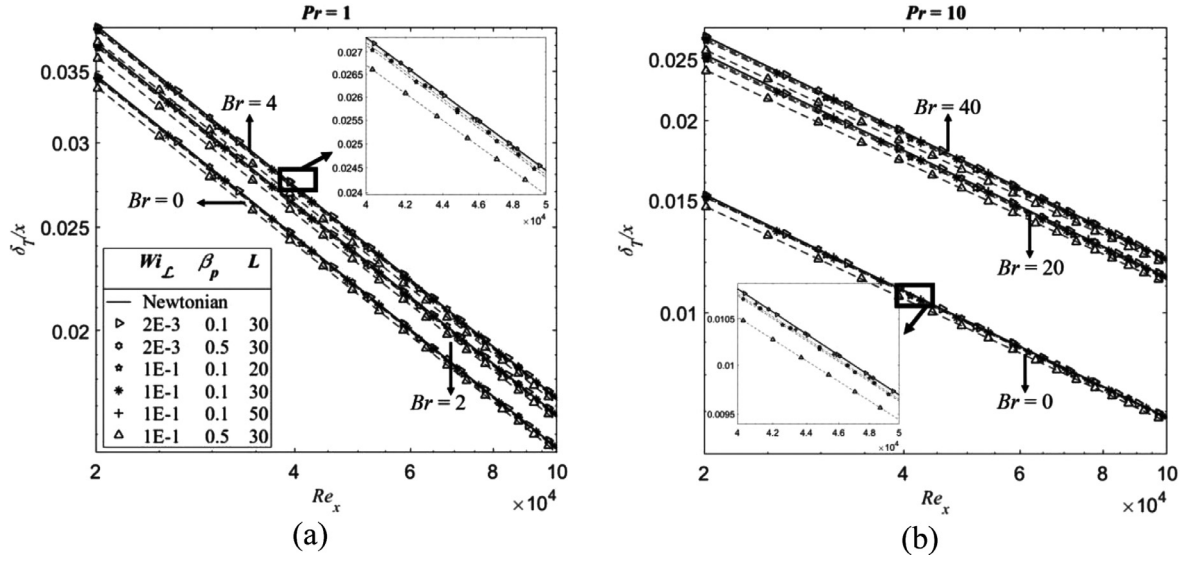

Fig. 9. Streamwise variation of the normalized thermal boundary layer thickness (δ_T/x) under various flow conditions for constant wall temperature with (a) Pr=1, (b) $Pr = 10$. The inset plots profiles for $4\times10^4 \le Re_x \le 5 \times 10^4$.

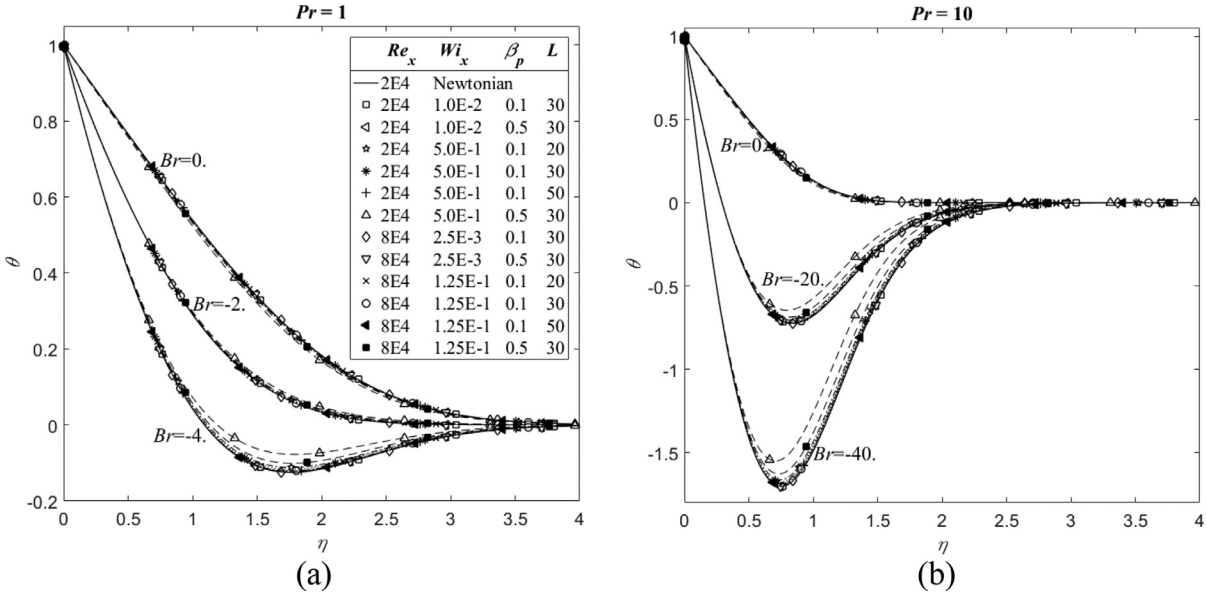

Fig. 10. Normalized transverse temperature profiles at $Re_x = 2 \times 10^4$ and 8×10^4 as a function of Reynolds number, Weissenberg number, viscosity ratio and dumbbell extensibility for constant wall temperature with (a) Pr=1, (b) $Pr = 10$.

between elasticity and viscous dissipation, so that increasing both enhances heat transfer (the shear-thinning nature of viscosity leads to sharper velocity variations near the wall). At larger Prandtl numbers, say $Pr = 10$, elasticity reduces the thickness of the thermal boundary layer in comparison with the corresponding Newtonian variation, both below and above Br_c. As discussed earlier the value of Br_c for $Pr = 10$ is rather low ($Br_c \cong -0.1$). The variation of the normalized thermal boundary layer thickness due to elasticity is of up to 10%.

5.2.3. Thermal boundary layer flow of FENE-P fluids with constant wall heat flux

(a) $q_w > 0$ (Fluid heating at the wall)

In this section the flow is heated by a constant wall heat flux. For constant wall heat flux cases the Brinkman number becomes a local quantity (Br_x) rather than global as for the constant wall temperature cases.

As shown in Fig. 13(a) and (b), when setting $Br_x = 0$ and elastic effects are weak, all solutions collapse onto the classical Newtonian solution. As viscous dissipation is increased, the dimensionless temperature profiles shift upward, because the fluid is warmer across the boundary layer. For this case of fluid heating at the wall the maximum dimensionless (and dimensional) temperature is always at the flat plate surface and the minimum temperature is in the free stream flow, regardless of the value of Br_x and all the heat has to be removed from the boundary layer by the free-stream. Increasing Br_x, with all other quantities fixed, increases the maximum value of the dimensionless temperature (at the wall). The temperature profiles at different levels of elasticity (but constant $Br_{\mathcal{L}}$) exhibit more separation from each other, i.e., the effect of elasticity is enhanced by viscous dissipation, but with elasticity reducing the values of θ. Viscous effects are always attenuated along the plate because of the way Br_x varies with x for a constant wall heat flux, according to Eq. (39), meaning that on going

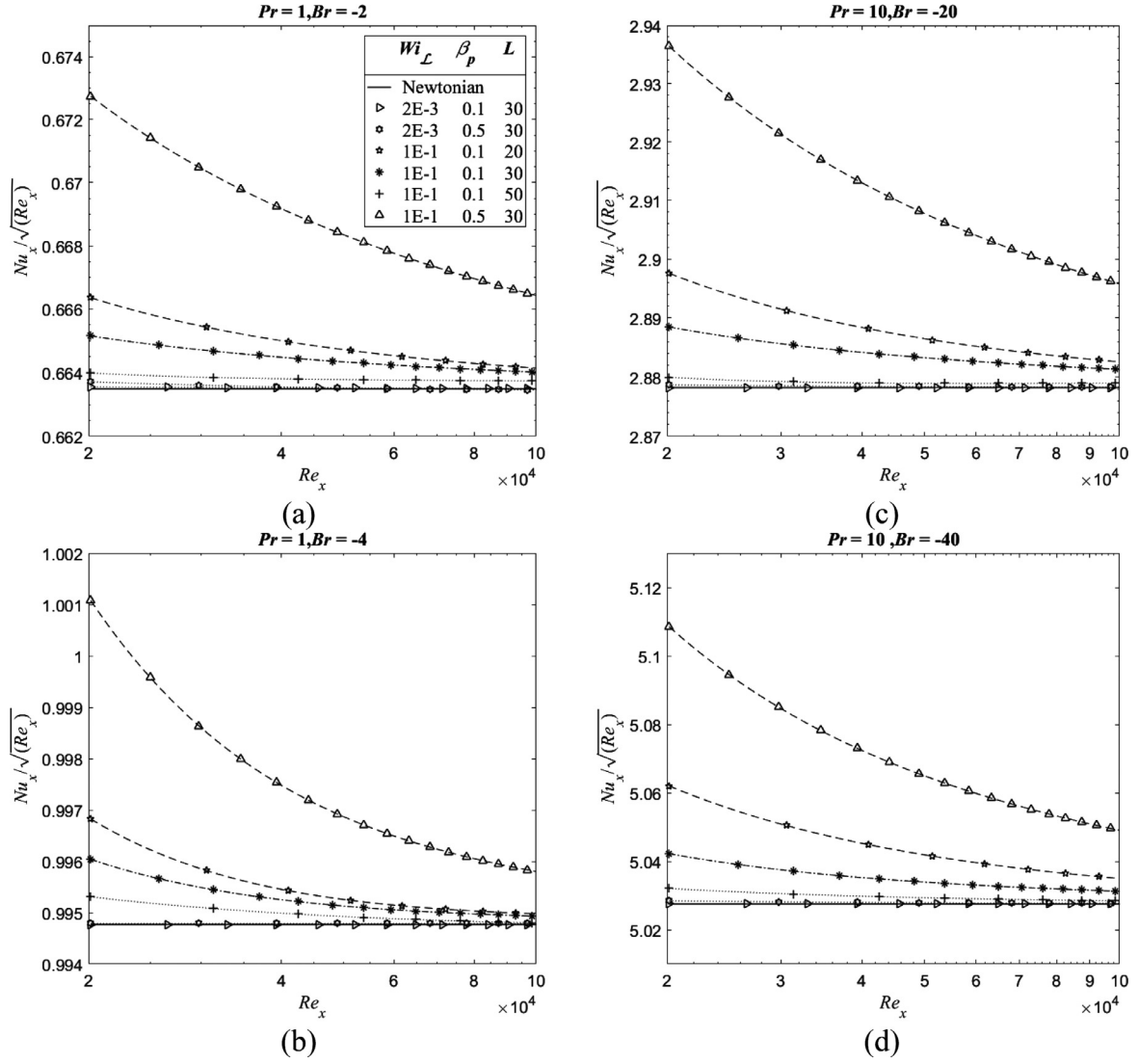

Fig. 11. Streamwise variation of the compensated Nusselt number ($Nu_x/\sqrt{Re_x}$) under various flow conditions for constant wall temperature with (a),(b) $Pr = 1$ and (c),(d) $Pr = 10$.

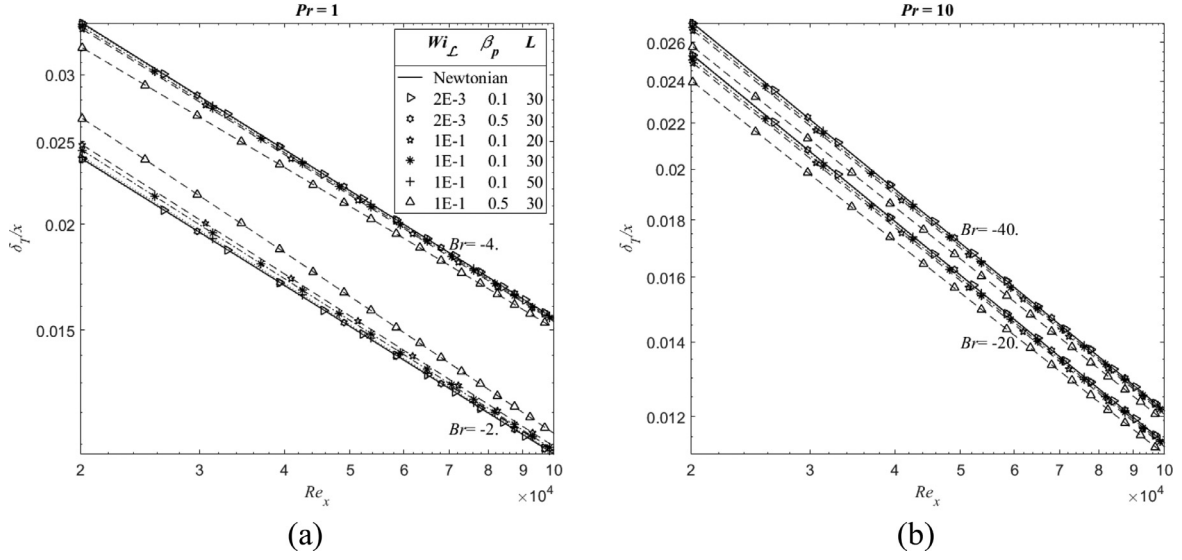

Fig. 12. Streamwise variation of the normalized thermal boundary layer thickness (δ_T/x) under various flow conditions for constant wall temperature with (a) Pr=1, (b) $Pr = 10$.

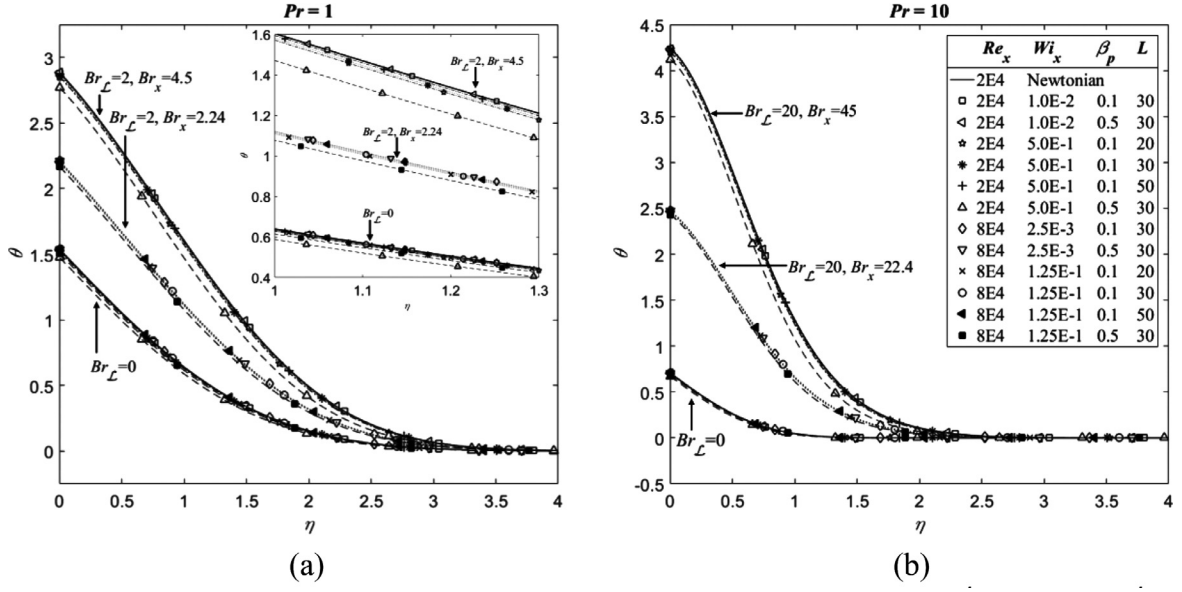

Fig. 13. Normalized transverse temperature profiles at $Re_x = 2 \times 10^4$ and 8×10^4 as a function of Reynolds number, Weissenberg number, viscosity ratio and dumbbell extensibility for constant wall heat flux with (a) Pr=1, (b) $Pr = 10$. The inset plots profiles for $1 \leq \eta \leq 1.3$.

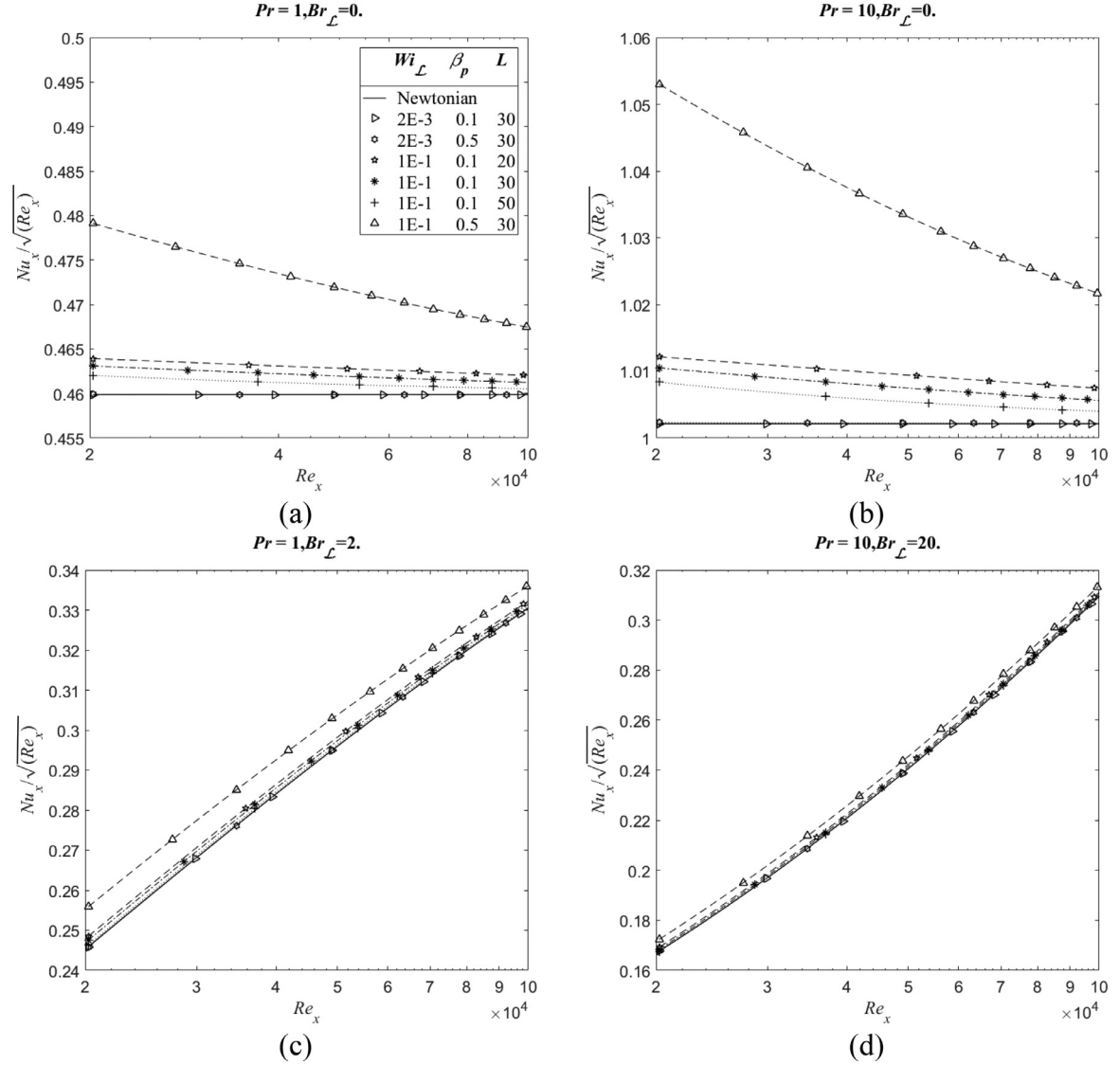

Fig. 14. Streamwise variation of the compensated Nusselt number ($Nu_x/\sqrt{Re_x}$) under various flow conditions for constant wall heat flux with (a)-(c) Pr=1 and (b)-(d) $Pr = 10$.

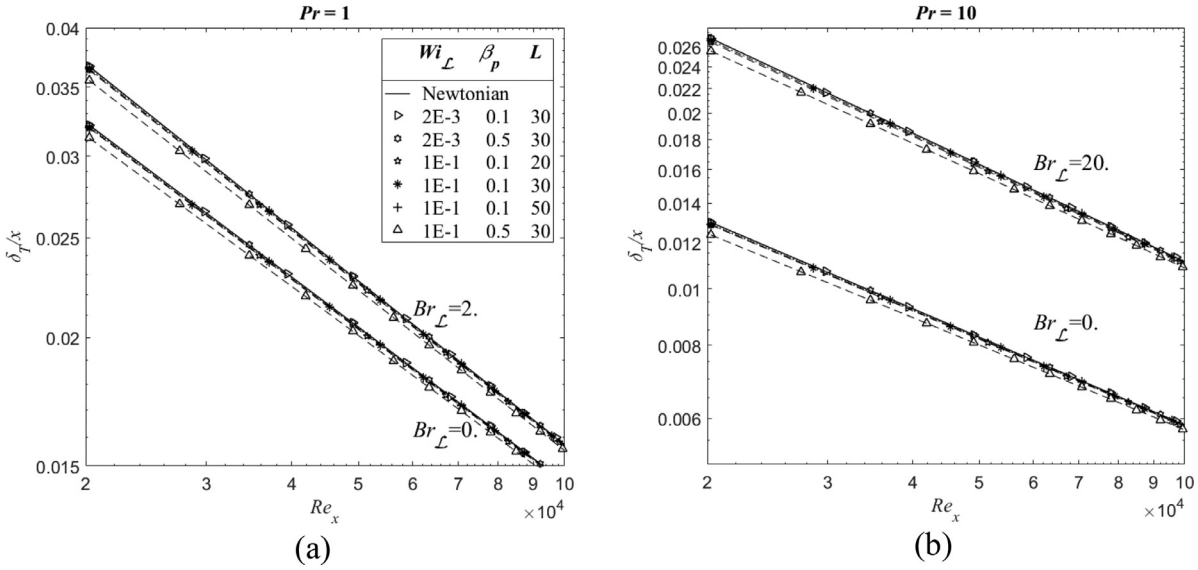

Fig. 15. Streamwise variation of the normalized thermal boundary layer thickness (δ_T/x) under various flow conditions for constant wall heat flux with (a) Pr=1, (b) $Pr = 10$.

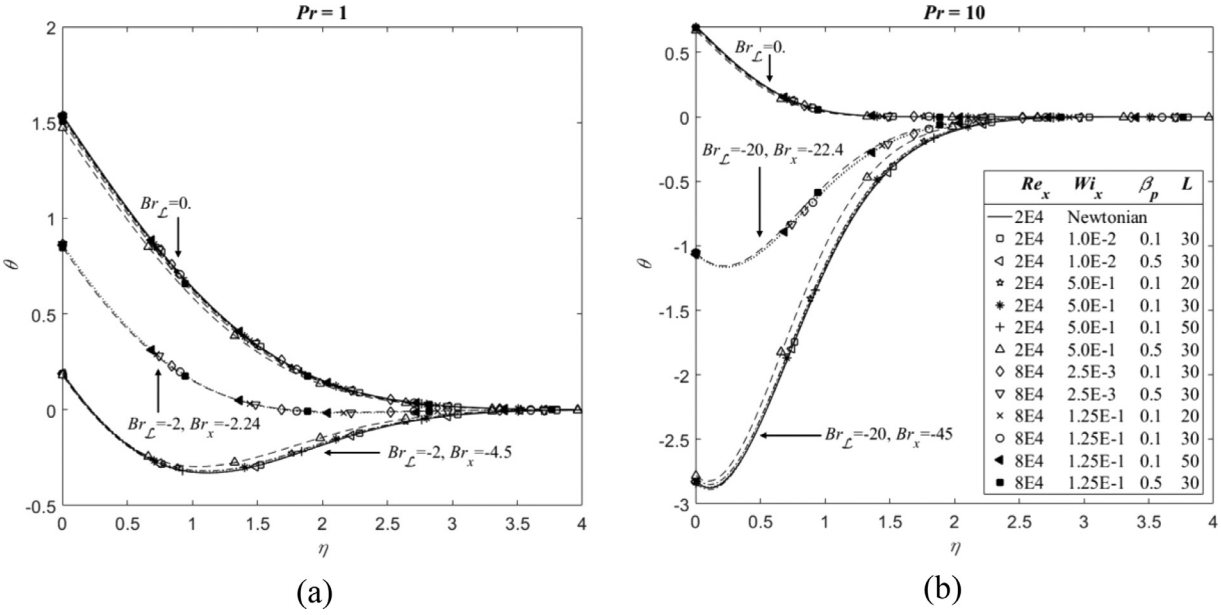

Fig. 16. Normalized transverse temperature profiles at $Re_x = 2 \times 10^4$ and 8×10^4 as a function of Reynolds number, Weissenberg number, viscosity ratio and dumbbell extensibility for constant wall heat flux with (a) Pr=1, and (b) $Pr = 10$.

downstream the viscous dissipation generates less heat, and consequently the maximum dimensionless temperature $\theta(x, 0)$, happening on the flat plate surface, is gradually reduced. To study the interplay of both elasticity and viscous dissipation, it is more enlightening to compare the normalized temperature curves at two different locations. For $Br_{\mathcal{L}} = 2$ and 20, the local Brinkman numbers are $Br_x = 4.5$ and 45 at $\frac{x}{\mathcal{L}} = 0.2$ with $Wi_x = 0.5$, and also $Br_x = 2.24$ and 22.4 at $\frac{x}{\mathcal{L}} = 0.8$ with $Wi_x = 0.125$, as shown in the upper and lower set curves in Fig. 13 (a),(b), respectively. As seen, by weakening both the viscous dissipation and elasticity effects in the streamwise direction the maximum deviation of θ between the largest elasticity level and the Newtonian curves is reduced from 5% to 2%, and from 3% to 1.5% for $Br_{\mathcal{L}} = 2$ and 20 respectively.

Fig. 14 (a),(b) show the effects of elasticity and viscous dissipation on the Nusselt number. In the absence of viscous dissipation, elasticity enhances heat transfer, with the effect decreasing along the plate because elastic effects decrease on going downstream. In the presence of viscous dissipation ($Br_{\mathcal{L}} > 0$) the Nusselt number is reduced in comparison with $Br_{\mathcal{L}} = 0$, because the wall heat flux and by implication the wall temperature gradient, remain fixed therefore the temperature difference between the wall and the free stream has to increase. Since there is an intense variation of the wall temperature along the plate, essentially due to the varying Br_x, the streamwise variation of $Nu_x/\sqrt{Re_x}$ becomes quite different and changes in slope relative to the case with negligible dissipation. As seen, elasticity increased the compensated Nusselt number by up to 5% and this deviation is further enhanced for larger Wi numbers.

The variations of the dimensionless thermal boundary layer thickness with flow elasticity, Brinkman and Reynolds numbers are shown in Fig. 15 (a),(b). As for the constant wall temperature cases, the thermal boundary layer thickens with Br and thins with elasticity regardless of the Prandtl number. Here, elasticity effect reduces δ_T/x by up to 5%.

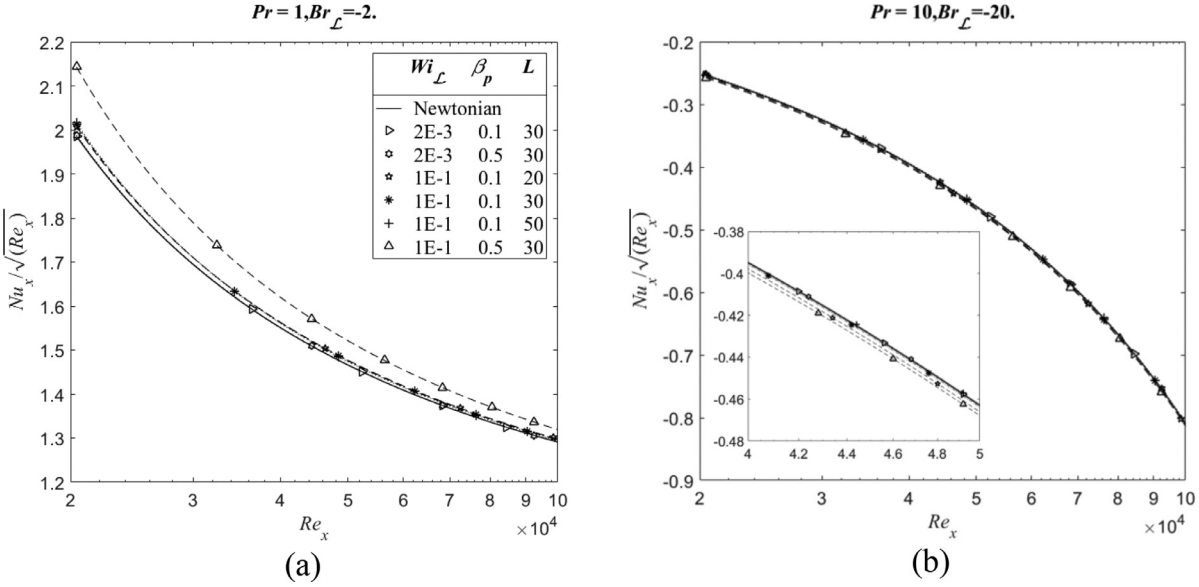

Fig. 17. Streamwise variation of the compensated Nusselt number ($Nu_x/\sqrt{Re_x}$) under various flow conditions for constant wall heat flux with (a) $Pr = 1$, (b) $Pr = 10$. The inset plots profiles for $4\times10^4 \leq Re_x \leq 5 \times 10^4$.

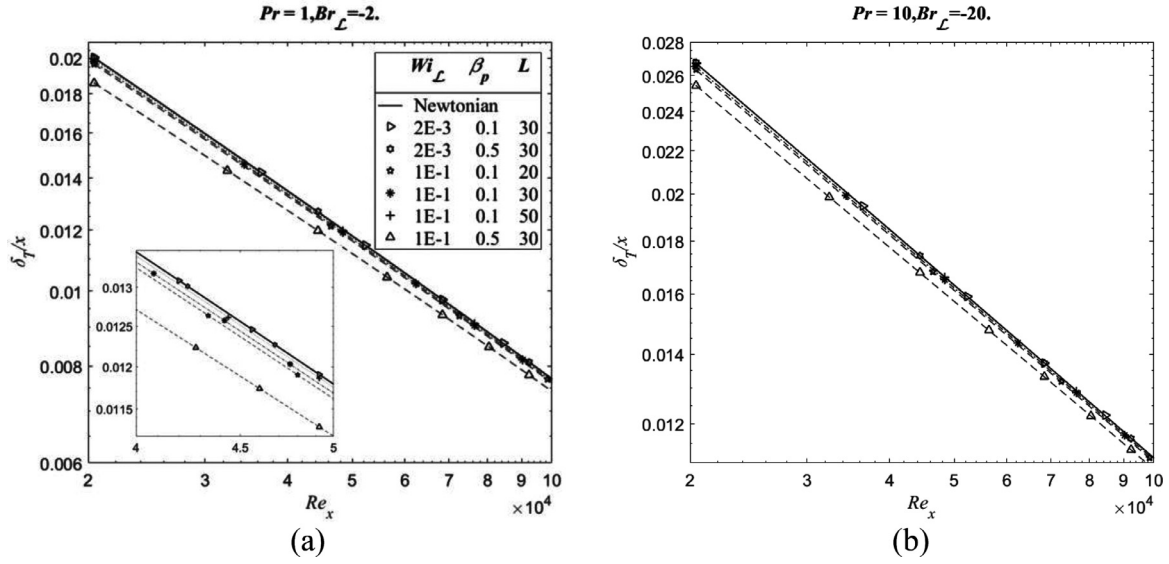

Fig. 18. Streamwise variation of the normalized thermal boundary layer thickness (δ_T/x) under various flow conditions for constant wall heat flux with (a) Pr=1, and (b) $Pr = 10$. The inset plots profiles for $4\times10^4 \leq Re_x \leq 5 \times 10^4$.

(**b**) $q_w < 0$ (Fluid cooling at the wall)

Cooling the thermal boundary layer at the wall with a constant heat flux is discussed here considering viscous dissipation and elastic effects. As for wall heating under constant wall temperature conditions, in the absence of viscous dissipation there is no difference between fluid cooling and heating at the wall in terms of dimensionless quantities. Similarly, viscous dissipation leads to a local definition of the Brinkman number (Br_x) as per Eq. (39).

However, and in contrast with the fluid wall heating case, as viscous dissipation becomes stronger than a critical value, a layer of fluid half way between the wall and the free stream becomes warmer than the free stream fluid so that such region starts to be cooled both by the wall and by the free stream flow. This is seen in the dimensionless temperature profiles of Fig. 16 (a) and (b) through the development of negative values of θ with the corresponding lower peak approaching the wall as Br increases in magnitude ($Br < 0$ for wall cooling, cf. Eq. (39)). At $Br_{\mathcal{L}} = 0$, i.e., no viscous dissipation, the maximum non-dimensional temperature is at the wall, and its minimum is outside the thermal boundary layer. However, by increasing the magnitude of the negative Brinkman number in the range of $-2 < Br_x < 0$ and generating more heat by viscous dissipation, the fluid warms and the maximum dimensionless temperature gradually reduces. For more negative Brinkman numbers the location of the maximum dimensionless temperature changes and takes place at the free stream region. In this situation, the minimum dimensionless temperature happens close to wall and its value decreases by decreasing $Br_{\mathcal{L}}$, indicating that the fluid is simultaneously being cooled by the wall and by the free stream flow. It is also observed that the elasticity causes the location of minimum dimensionless temperature shift slightly toward the wall. As shown, viscous dissipation increases the impact of elasticity upon the temperature profiles, i.e., for the same value of $Br_{\mathcal{L}}$ the curves of θ show a wider spread than at larger values of $|Br_x|$. The interaction of elasticity and viscous dissipation effects on normalized temperature is shown at two dif-

ferent locations. For $Br_{\mathcal{L}} = -2$ and -20 cases, the local Brinkman numbers are $Br_x = -4.5$ and -45 at $\frac{x}{\mathcal{L}} = 0.2$ with $Wi_x = 0.5$, and also $Br_x = -2.24$ and -22.4 at $\frac{x}{\mathcal{L}} = 0.8$ with $Wi_x = 0.125$, as shown by upper and lower set curves, respectively in Fig. 16 (a),(b). As shown, the effects of elasticity and of viscous dissipation are attenuated by increasing the distance from the leading edge of the flat plate, therefore the maximum variation of θ for the largest elasticity level and relative to the Newtonian curves decrease from 10% to 3%, and from 20% to 7% for $Br_{\mathcal{L}} = -2$ and -20, respectively.

Fig. 17 (a),(b) confirm that the effect of elasticity on Nusselt number depends also on the viscous dissipation magnitude. As displayed for Pr=1 and $Br_{\mathcal{L}} = -2$ in Fig. 17 (a), the Nusselt number decreases in the streamwise direction and increases with flow elasticity in this range. However, by enhancing viscous dissipation, as measured by $Br_{\mathcal{L}} = -20$, the Nusselt number changes sign (cf. its definition in Eq. (48)) and its absolute value now increases in the streamwise direction. Increasing flow elasticity also slightly increases the absolute value of Nu, as shown in Fig. 17 (b) for Pr=10. Looking at the variation of the absolute value of the compensated Nusselt number, it is observed that increasing elasticity always enhances heat transfer: this is seen as an increment in $|Nu_x/\sqrt{Re_x}|$ of up to 8% and 3% for $Br_{\mathcal{L}} = -2$ and -20, respectively.

Fig. 18 (a),(b) displays the corresponding effects on the thermal boundary layer thickness variation. As shown, the thermal boundary layer thickens with viscous dissipation, whereas flow elasticity has the opposite effect. Here, the elasticity effect leads up to 10 % decrement of (δ_T/x).

6. Conclusions

Using boundary layer arguments an order of magnitude analysis of the governing equations for the steady, two-dimensional, laminar boundary layer flow of FENE-P fluids with temperature-independent properties is carried out for two independent thermal conditions, namely for a constant wall temperature and for a constant wall heat flux. Each thermal case leads to a semi-analytical solution of the thermal energy equation which is mathematically an approximate self-similar solution with a local nature, i.e., exhibiting a dependence on the local streamwise coordinate. However, under conditions of low elasticity, the normalized flow characteristics show a global-like self-similar behavior with kinematic quantities collapsing on the corresponding Newtonian self-similar result and with polymer-based quantities collapsing also onto single self-similar curves. As elasticity levels increase, by taking on larger values of Wi_x and β_p and/or low values of L, there is a progressive deviation from the low elasticity asymptotic profiles.

The comparisons showed that the present solution predicts the normalized transverse temperature profiles, thermal boundary layer thickness, and Nusselt number with an excellent agreement with RheoFoam simulations in the absence and with viscous dissipation effects (e.g. Br=4). In addition, the comparison between the present solution with Olagunju's work for $Wi \approx 1$ (Wi_x= 1.0) and $Br = 4$ also revealed that Olagunju's solution accuracy is lower than that of our solution for predicting flow properties. Through a comparison with the numerical solution of the full set of governing equations, performed by RheoFoam, it was found that the semi-analytical solution is valid up to local Weissenberg numbers (Wi_x) of Wi_x= 5.0, beyond which differences exceed 5%.

The effects of viscous dissipation and elasticity on Nusselt numbers for various heating and cooling conditions with constant wall temperature and constant heat flux conditions are comprehensively studied and reported. For both conditions, it is observed that at low elasticity levels the local Nusselt number (Nu_x) is similar to the Newtonian value. However, the Nusselt number increases with elasticity and for a given set of flow and thermal conditions, the compensated Nusselt number ($Nu_x/\sqrt{Re_x}$) ceases to be constant and decreases non-linearly along the plate towards the Newtonian constant value. In any case it is worth noting that for all cases studied, larger viscous dissipation strengthens the elasticity effect.

The effects of viscous dissipation and elasticity on the variations of the thermal boundary layer thickness (δ_T/x) are also presented. At low elasticity δ_T/x follows the corresponding Newtonian behavior, but on increasing elasticity levels the thermal boundary layer thins by up to 10% for the cases studied. In contrast, the enhancement of viscous dissipation thickens the thermal boundary layer, especially for Brinkman numbers above the critical value at which the temperature inside the boundary layer exceeds the wall temperature or the free-stream temperature.

Declaration of Competing Interest

The authors declare that they have no known competing financial interests or personal relationships that could have appeared to influence the work reported in this paper.

CRediT authorship contribution statement

Saeed Parvar: Conceptualization, Methodology, Software, Validation, Formal analysis, Investigation, Data curation, Writing – original draft. **Carlos B. da Silva:** Writing – review & editing, Supervision, Project administration, Funding acquisition. **Fernando Pinho:** Methodology, Resources, Writing – review & editing, Supervision, Project administration, Funding acquisition.

Acknowledgments

The authors acknowledge the financial support of project PTDC/EMS-ENE/2390/2014, POCI-01–0145-FEDER-016669 funded by Fundo Europeu de Desenvolvimento Regional, via COMPETE2020 - Programa Operacional Competitividade e Internacionalização (POCI) and Fundação para a Ciência e a Tecnologia. In addition, S. P. and F. T. P. are grateful to Centro de Estudos de Fenómenos de Transporte for funding through projects UIDB/00532/2020 and UIDP/00532/2020. C.B.d.S. acknowledges Fundação para a Ciência e Tecnologia (FCT) through IDMEC, under LAETA, project UIDB/50022/2020.

References

[1] B.A. Toms, Some observations on the flow of linear polymer solutions through straight tubes at large Reynolds numbers, in: Proceedings of the 1st International Congress on Rheologys, 2, North-Holland, Amsterdam, 1949, p. 135.
[2] A. Leca, M. Leca, Drag reduction and heat transfer measurements with polyacrylamides on a model of a district heating system, in: Proceedings of the 3rd International Conference on Drag Reduction, Bristol, 1984 2-5 July.
[3] E.F. Matthys, Heat transfer, drag reduction, and fluid characterization for turbulent flow of polymer solutions: recent results and research needs, J. Non Newton. Fluid Mech. 38 (1991) 313–342, doi:10.1016/0377-0257(91)83010-2.
[4] M. Kostic, On turbulent drag and heat transfer reduction phenomena and laminar heat transfer enhancement in non-circular duct flow of certain non-Newtonian fluids, Int. J. Heat Mass Transf. 37 (1) (1994) 133–147 Supplement, doi:10.1016/0017-9310(94)90017-5.
[5] G. Ahlers, A. Nikolaenko, Effect of a polymer additive on heat transport in turbulent Rayleigh-Benard convection, Phys. Rev. Lett. 104 (2010) 034503, doi:10.1103/PhysRevLett.104.034503.
[6] Y. Wang, B. Yu, J.L. Zakin, H Shi, Review on drag reduction and its heat transfer by additives, Adv. Mech. Eng. 3 (17) (2011) 478749, doi:10.1155/2011/478749.
[7] P. Wei, N. Rui, K. Xia, Enhanced and reduced heat transport in turbulent thermal convection with polymer additives, Phys. Rev. E 86 (2012) 016325, doi:10.1103/PhysRevE.86.016325.
[8] A.N. Beris, B.J. Edwards, Thermodynamics of Flowing Systems, Thermodynamics of Flowing Systems: with Internal Microstructure, Oxford Science Publication, New York, May 1994 1st printing.
[9] R.B. Bird, R.C. Armstrong, O. Hassager, Dynamics of Polymeric Liquids, Vol. 1: Fluid Mechanics, 2nd ed., Wiley, New York, 1987.
[10] J.M. Nóbrega, F.T. Pinho, P.J. Oliveira, O.S. Carneiro, Accounting for temperature-dependent properties in viscoelastic duct flows, Int. J. Heat Mass Transf. 47 (6–7) (2004) 1141–1158, doi:10.1016/j.ijheatmasstransfer.2003.10.004.

[11] F. Pimenta, M.A. Alves, Conjugate heat transfer in the unbounded flow of a viscoelastic fluid past a sphere, Int. J. Heat Fluid Flow 89 (2021) 108784, doi:10.1016/j.ijheatfluidflow.2021.108784.
[12] M. Massoudi, Local non-similarity solutions for the flow of a non-Newtonian fluid over a wedge, Int. J. Non Linear Mech. 36 (6) (2001) 961–976, doi:10.1016/S0020-7462(00)00061-5.
[13] W.A. Khan, J.R. Culham, M.M. Yovanovich, Fluid flow and heat transfer in power-law fluids across circular cylinders: analytical study, ASME J. Heat Transf. 128 (9) (2006) 870–878, doi:10.1115/1.2241747.
[14] H. Shokouhmand, M. Soleimani, The effect of viscous dissipation on temperature profile of a power-law fluid flow over a moving surface with arbitrary injection/suction, Energy Convers. Manag. 52 (1) (2011) 171–179, doi:10.1016/j.enconman.2010.06.056.
[15] A. Barletta, Fully developed laminar forced convection in circular ducts for power-law fluids with viscous dissipation, Int. J. Heat Mass Transf. 40 (1) (1996) 15–26, doi:10.1016/S0017-9310(96)00094-4.
[16] C.P. Tso, J. Sheela-Francisca, H. Yew-Mun, Viscous dissipation effects of power-law fluid flow within parallel plates with constant heat fluxes, J. Non Newton. Fluid Mech. 165 (2010) 625–630, doi:10.1016/j.jnnfm.2010.02.023.
[17] J. Sheela-Francisca, C.P. Tso, H. Yew-Mun, D. Rilling, Heat transfer on asymmetric thermal viscous dissipative Couette-Poiseuille flow of pseudo-plastic fluids, J. Non Newton. Fluid Mech. 169–170 (2012) 42–53, doi:10.1016/j.jnnfm.2011.11.005.
[18] D.O. Olagunju, A self-similar solution for forced convection boundary layer flow of a FENE-P fluid, Appl. Math. Lett. 19 (2006) 432–436, doi:10.1016/j.aml.2005.05.015.
[19] R. Benzi, E. Ching, V. Chu, Heat transport by laminar boundary layer flow with polymers, J. Fluid Mech. 696 (2012) 330–344, doi:10.1017/jfm.2012.46.
[20] R. Benzi, E. Ching, W. Yu, Y. Wang, Heat transport modification by finitely extensible polymers in laminar boundary layer flow, J. Fluid Mech. 788 (2016) 337–357, doi:10.1017/jfm.2015.714.
[21] Cebeci T., Bradshaw P., Physical and Computational Aspects of Convective Heat Transfer, Springer-Verlag Berlin Heidelberg. doi:10.1007/978-1-4612-3918-5.
[22] E.M. Sparrow, H. Quack, C.J. Boerner, Local nonsimilarity boundary-layer solutions, AIAA J. 8 (11) (1970) 1936–1942, doi:10.2514/3.6029.
[23] E.M. Sparrow, H.S Yu, Local non-similarity thermal boundary-layer solutions, ASME J. Heat Transf. 93 (4) (1971) 328–334, doi:10.1115/1.3449827.
[24] T.Y. Na, Computational Methods in Engineering Boundary Value Problems, Academic Press, New York, 1979.
[25] R. Seshadri, T.Y. Na, Group Invariance in Engineering Boundary Value Problems, Springer, New York, 1985.
[26] A. Ishak, R. Nazar, I. Pop, D. Kapur, Local similarity solutions for laminar boundary layer flow along a moving cylinder in a parallel stream eds, Computer Mathematics: ASCM 2007. Lecture Notes in Computer Science, 5081, Springer, Berlin, Heidelberg, 2008, doi:10.1007/978-3-540-87827-8_19.
[27] A. Peterlin, Streaming birefringence of soft linear macromolecules with finite chain length, Polymer 2 (1961) 257–264, doi:10.1016/0032-3861(61)90029-5.
[28] R.B. Bird, P.J. Dotson, N.L. Johnson, Polymer solution rheology based on a finitely extensible bead-spring chain model, J. Non Newton. Fluid Mech. 7 (1980) 213–235, doi:10.1016/0377-0257(80)85007-5.
[29] F.T. Pinho, P.M. Coelho, Fully-developed heat transfer in annuli for viscoelastic fluids with viscous dissipation, J. Non Newton. Fluid Mech. 138 (2006) 7–21, doi:10.1016/j.jnnfm.2006.04.002.
[30] P.M. Coelho, F.T. Pinho, P.J. Oliveira, Fully developed forced convection of the Phan-Thien-Tanner fluid in ducts with a constant wall temperature, Int. J. Heat Mass Transf. 45 (2002) 1413–1423, doi:10.1016/S0017-9310(01)00236-8.
[31] P.J. Oliveira, An exact solution for tube and slit flow of a FENE-P fluid, Acta Mech. 158 (2002) 157–167, doi:10.1007/BF01176906.
[32] K.R. Rajagopal, A.S. Gupta, T.Y. Na, A note on the Falkner-Skan flows of a non-Newtonian fluid, Int. J. Non Linear Mech. 18 (4) (1983) 313–320, doi:10.1016/0020-7462(83)90028-8.
[33] D.O. Olagunju, Local similarity solutions for boundary layer flow of a FENE-P fluid, Appl. Math. Comput. 173 (2006) 593–602 a, doi:10.1016/j.amc.2005.04.051.
[34] H. Blasius, Grenzschichten in Flüssigkeiten mit kleiner Reibung, Z. Angew. Math. Phys. 56 (1908) 1–37 http://naca.central.cranfield.ac.uk/reports/1950/naca-tm-1256.pdf. as assessed on 30th July 2020.
[35] S. Parvar, C.B. da Silva, F.T. Pinho, Local similarity solution for steady laminar planar jet flow of viscoelastic FENE-P fluids, J. Non Newton Fluid Mech. 279 (2020) 104265, doi:10.1016/j.jnnfm.2020.104265.
[36] S. Parvar, C.B. da Silva, F.T. Pinho, Corrigendum to “local similarity solution for steady laminar planar jet flow of viscoelastic FENE-P fluids” [Journal of Non-Newtonian Fluid Mechanics 279 (2020) 104265], J. Non Newton. Fluid Mech. 281 (2020) 104309, doi:10.1016/j.jnnfm.2020.104309.
[37] S. Parvar, C.B. da Silva, F.T. Pinho, Revisiting the laminar boundary layer flow of viscoelastic FENE-P fluids, Phys. Fluids 33 (2021) 023103, doi:10.1063/5.0042516.
[38] F.M. White, Viscous Fluid Flow, 3rd ed., McGraw Hill, 2006.
[39] H. Schlichting, K. Gersten, Boundary-Layer Theory, 8th Revised and Enlarged Edition, McGraw Hill, 1999.
[40] F. Pimenta, M. Alves, Stabilization of an open-source finite-volume solver for viscoelastic fluid flows, J. Non Newton. Fluid Mech. 239 (2017) 85–104, doi:10.1016/j.jnnfm.2016.12.002.
[41] Pimenta F., and Alves M.A., rheoTool, https://github.com/fppimenta/rheoTool, (2016).
[42] R.B. Bird, C.F. Curtiss, R.C. Armstrong, O. Hassager, Dynamics of Polymeric Fluids. Vol. 2: Kinetic Theory, 2nd ed., Wiley, New York, 1987.
[43] T Vaithianathan, LR Collins, Numerical approach to simulating turbulent flow of a viscoelastic polymer solution, J. Comput. Phys. 187 (2003) 1–21, doi:10.1016/S0021-9991(03)00028-7.
[44] P.C. Valente, C.B. da Silva, F.T. Pinho, The effect of viscoelasticity on the turbulent kinetic energy cascade, J. Fluid Mech. 760 (2014) 39–62, doi:10.1017/jfm.2014.585.
[45] C.F. Li, V.K. Gupta, R. Sureshkumar, B. Khomami, Turbulent channel flow of dilute polymeric solutions: drag reduction scaling and an eddy viscosity model, J. Non Newton. Fluid Mech. 139 (2006) 177–189, doi:10.1016/j.jnnfm.2006.04.012.
[46] M.C. Guimarães, N. Pimentel, F.T. Pinho, C.B. da Silva, Direct numerical simulations of turbulent viscoelastic jets described by the FENE-P model, J. Fluid Mech. 899 (A11) (2020), doi:10.1017/jfm.2020.402.
[47] P.O. Ferreira, F.T. Pinho, C.B. da Silva, Large-eddy simulations of forced isotropic turbulence with viscoelastic fluids described by the FENE-P model, Phys. Fluids 28 (2016) 125104, doi:10.1063/1.4968218.
[48] S. Parvar, C.B. da Silva, F.T. Pinho, Large eddy simulations of turbulent planar jets of viscoelastic fluids, Phys. Fluids 33 (2021) 045110, doi:10.1063/5.0039826.
[49] M. Masoudian, F.T. Pinho, K. Kim, R. Sureshkumar, A viscoelastic k-ε-v2-f turbulent flow model valid up to the maximum drag reduction limit, J. Non Newton. Fluid Mech. 202 (2013) 99–111, doi:10.1016/j.jnnfm.2013.09.007.
[50] M. Masoudian, F.T. Pinho, K. Kim, R. Sureshkumar, A Reynolds stress model for turbulent flow of homogeneous polymer solutions, Int. J. Heat Fluid Flow 54 (2015) 220–235, doi:10.1016/j.ijheatfluidflow.2015.05.017.
[51] M. Masoudian, F.T. Pinho, K. Kim, R. Sureshkumar, A RANS model for heat transfer reduction in viscoelastic turbulent flow, Int. J. Heat Mass Transf. 100 (2016) 332–346, doi:10.1016/j.ijheatmasstransfer.2016.04.053.
[52] G.W.M. Peters, F.P.T. Baaijens, Modelling of non-isothermal viscoelastic flows, J. Non Newton. Fluid Mech. 68 (1997) 205–224, doi:10.1016/S0377-0257(96)01511-X.
[53] G.C. Sarti, N. Esposito, Testing thermodynamic constitutive equations for polymers by adiabatic deformation experiments, J. Non Newton. Fluid Mech. 3 (1977/78) (2002) 65–76, doi:10.1016/0377-0257(77)80012-8.
[54] A. Wachs, J.R. Clermont, Non-isothermal viscoelastic flow computations in an axisymmetric contraction at high Weissenberg numbers by a finite volume method, J. Non Newton. Fluid Mech. 95 (2000) 147–184, doi:10.1016/S0377-0257(00)00176-2.
[55] S. Parvar, C.B. da Silva, F.T. Pinho, The steady laminar planar mixing layer flow of viscoelastic FENE-P fluids, J. Eng. Math. (2021), doi:10.1007/s10665-021-10191-7.
[56] A. Bejan, Convection Heat Transfer, 4th ed., John Wiley & Sons, 2013.
[57] L. Edberg, Introduction to Computation and Modeling For Differential Equations, 2nd ed, John Wiley & Sons, Inc., Hoboken, New Jersey, 2016.
[58] W.H. Press, S.A. Teukolsky, W.T. Vetterling, B.P. Flannery, Numerical Recipes, The Art of Scientific Computing, 3rd ed, Cambridge Press, 2007.
[59] G. Birkhoff, S. MacLane, A.K Peters, A Survey of Modern Algebra (Akp Classics), 5th ed, CRC Press, 1998.
[60] Madureira A (1948) Lessons in Algebra and Analytical Geometry. Volume 1 – Algebra (in Portuguese), 2nd edition, Porto Editora, Porto, Portugal.
[61] M.A. Alves, P.J. Oliveira, F.T. Pinho, A convergent and universally bounded interpolation scheme for the treatment of advection, Int. J. Numer. Methods Fluids 41 (2003) 47–75, doi:10.1002/fld.428.